DELAYED REACTION-KINETICS AND THE STABILITY OF SPIKES IN THE GIERER-MEINHARDT MODEL

NABIL T. FADAI*, MICHAEL J. WARD†, AND JUNCHENG WEI‡

Abstract. A linear stability analysis of localized spike solutions to the singularly perturbed two-component Gierer-Meinhardt (GM) reaction-diffusion (RD) system with a fixed time-delay T in the nonlinear reaction-kinetics is performed. Our analysis of this model is motivated by the computational study of Seirin Lee et al. (2010) [13] on the effect of gene expression time delays on spatial patterning for both the GM model and some related RD models. It is shown that the linear stability properties of such localized spike solutions are characterized by the discrete spectra of certain nonlocal eigenvalue problems (NLEP). Phase diagrams consisting of regions in parameter space where the steady-state spike solution is linearly stable are determined for various limiting forms of the GM model in both 1-D and 2-D domains. On the boundary of the region of stability, the spike solution is found to undergo a Hopf bifurcation. For a special range of exponents in the nonlinearities for the 1-D GM model, and assuming that the time-delay only occurs in the inhibitor kinetics, this Hopf bifurcation boundary is readily determined analytically. For this special range of exponents, the challenging problem of locating the discrete spectrum of the NLEP is reduced to the much simpler problem of locating the roots to a simple transcendental equation in the eigenvalue parameter. By using a hybrid analytical-numerical method, based on a parametrization of the NLEP, it is shown that qualitatively similar phase diagrams occur for general GM exponent sets and for the more biologically relevant case where the time-delay occurs in both the activator and inhibitor kinetics. Overall, our results show that there is a critical value $T_\star$ of the delay for which the spike solution is unconditionally unstable for $T > T_*$, and that the parameter region where linear stability is assured is, in general, rather limited. A comparison of the theory with full numerical results computed from the RD system with delayed reaction-kinetics for a particular parameter set suggests that the Hopf bifurcation can be subcritical, leading to a global breakdown of a robust spatial patterning mechanism.

1. Introduction. In [20], Alan Turing proposed that localized peaks in the concentration of a chemical substance, known as a morphogen, could be responsible for the process of morphogenesis, which describes the development of a complex organism from a single cell. Through the use of a linearized analysis, he showed how stable spatially complex patterns can develop from small perturbations of spatially homogeneous initial data for a coupled two-component system of reaction-diffusion (RD) equations. Although there is now a vast literature on the study of Turing pattern formation for specific RD systems proposed to model various morphogenetic processes (cf. [5] and the references therein), these previous studies have typically neglected any time-delays in the reaction kinetics owing to the time needed for gene expression. More specifically, as discussed in [5], there may exist a time-delay between the initiation of protein signal transduction, due to ligand-receptor binding, and the time at which genes are ultimately produced.

In [5], [13], [14], [15] (see also the survey [17]), the effect of a fixed time-delay in the reaction-kinetics for some Turing pattern formation systems, modeling various hypothetical sub-cellular gene expression dynamical processes, was studied computationally and through a Turing-type linear stability analysis on both fixed and slowly growing domains. Each of the two-component RD models studied in [5], [13], [14], and [15] is characterized by a short-range activation and a long-range inhibition, with the Gierer-Meihnardt (GM) RD model being one such prototypical system [6]. In [13], a GM model with a time-delayed reaction-kinetics, modeling a signal transduction process involving reversible binding at the cell surface, was studied numerically (this is Model I in [13]). This computational study [13] showed that temporal oscillations in the spatial patterning occur as the time-delay increases, and that these oscillations become large and uncontrolled as the delay increases further. The main goal of this paper is provide a theoretical framework to predict parameter ranges where stable spatial patterning exists for this GM model of [13] with delayed reaction-kinetics.

In one spatial dimension, the dimensionless GM RD model [6] allowing for delayed reaction-kinetics (Model I of [13]), and posed on $|x| \le 1$ with $u_x(\pm 1, t) = v_x(\pm 1, t) = 0$, is

$$v_t = \varepsilon^2 v_{xx} - v + v_T^p/u_T^q\,, \qquad \tau u_t = D u_{xx} - u + \varepsilon^{-1} v_T^m/u_T^s\,, \tag{1.1a}$$

*Dept. of Mathematics, UBC, Vancouver, Canada, and OCIAM, Oxford University, Oxford, UK
†Dept. of Mathematics, UBC, Vancouver, Canada. (corresponding author ward@math.ubc.ca)
‡Dept. of Mathematics, UBC, Vancouver, Canada.

where $u_T \equiv u(x,t-T)$, $v_T \equiv v(x,t-T)$, $0<\varepsilon^2 \ll 1$ is the activator diffusivity, $D>0$ is the inhibitor diffusivity, and $\tau>0$ is a reaction-time constant. We assume the usual condition (cf. [11]) on the exponents (p,q,m,s) that

$$p>1\,, \qquad q>0\,, \qquad m>1\,, \qquad s\geq 0\,, \qquad \xi \equiv \frac{qm}{p-1}-s-1>0\,. \tag{1.1b}$$

In the semi-strong regime where $\epsilon \ll 1$ and $D=\mathcal{O}(1)$, and in the absence of delayed kinetics, there is a large literature on the stability of localized 1-D spike solutions to the GM model (1.1) (cf. [24], [4], [10], [11], [23], [22], [21]). To analyze the linear stability of a steady-state spike solution to $\mathcal{O}(1)$ time-scale instabilities, the main technical challenge is that one must rigorously analyze the discrete spectrum of a nonlocal eigenvalue problem (NLEP). Although there are many rigorous results on the spectrum of the NLEP for various ranges of the exponent set (p,q,m,s) (see the survey [25]), the theory is still incomplete. More recently, in [19] it was shown that when $p=2m-3$ and $m>2$ the study of the spectrum of the NLEP for the 1-D undelayed GM model (1.1) can be reduced to the analysis of a simple transcendental equation in the eigenvalue parameter. For this parameter range $p=2m-3$ with $m>2$, where we refer to the NLEP as being "explicitly solvable", detailed results for the linear stability of 1-D spike solutions are readily obtained. The specific case $p=m=3$ also arises in the study of the stability of hot-spot patterns for a RD model of urban crime (cf. [12]).

Motivated by the previous computational studies (cf. [5], [13], [14], [15]) of spatial patterning for the GM and related models with delayed reaction-kinetics, the main goal of this paper is to analyze the linear stability of steady-state spike solutions for (1.1) and its 2-D counterpart when the reaction-kinetics have a time delay T. For various limiting forms of (1.1), as we discuss below, our main focus is to determine a phase diagram in the τ versus T parameter space where the spike solution is linearly stable. On the boundary of the region of stability the spike solution undergoes a Hopf bifurcation. In our analysis, we will consider only $\mathcal{O}(1)$ time-scale instabilities associated with unstable spectra of the associated NLEP, which is obtained by linearizing (1.1) and its 2-D counterpart around a steady-state spike solution. In the 1-D case, and under the assumption of a delay only in the inhibitor kinetics, we will show that the NLEP stability analysis becomes highly tractable analytically for the parameter range $p=2m-3$ with $m>2$.

From a mathematical viewpoint, most previous studies of the effect of time-delayed reaction-kinetics on RD systems have focused on characterizing the linear stability of spatially uniform steady-states. In particular, rigorous results regarding the linear stability of the spatially uniform state for a general class of two-component RD system under time-delayed reaction-kinetics were established in [2] (see also the references therein). In addition, for a GM model with saturated and time-delayed reaction-kinetics, it was proved in [1] that the spatially uniform state is globally attractive when the saturation parameter is sufficiently large. In contrast to these previous studies regarding the spatially uniform steady-state, to our knowledge there has been no prior analytical studies of the linear stability of spike-type solutions to singularly perturbed RD systems with delayed reaction-kinetics.

A detailed outline of this paper is as follows. In §2 we study the linear stability of a one-spike solution to (1.1) in the shadow limit $D\to\infty$ (cf. [22]) under the assumption that the delay occurs only in the inhibitor. In the limit $T\to\infty$ of large delay, we show in §2.1 that there are branches of spectra for the NLEP in the unstable right-half plane $\mathrm{Re}(\lambda)>0$ that tend to origin $\lambda=0$ as $T\to\infty$. For the subrange of exponents $p=2m-3$ with $m>2$ for which the NLEP is explicitly solvable, in §2.2 we give an explicit determination of the Hopf bifurcation boundary in the τ versus T plane that forms the edge of the region in parameter space where the spike solution is linearly stable. For the corresponding shadow problem in N-spatial dimensions, and with an arbitrary GM exponent set, in §2.3 we show how to readily compute the Hopf bifurcation boundary in the τ versus T plane. In particular, in the left panel of Fig. 1.1, we plot the Hopf bifurcation boundary and the region of linear stability for the 1-D shadow problem for the prototypical GM exponent set

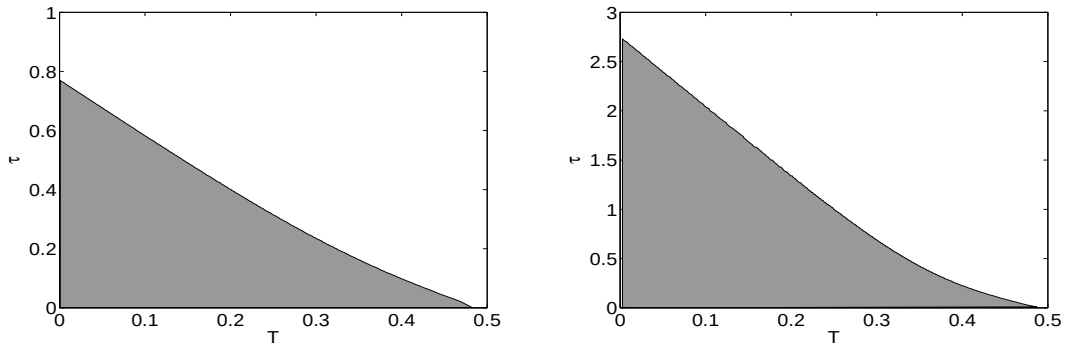

Fig. 1.1: The stable shaded region in the τ versus T plane for a one-spike solution to the shadow GM problem (2.1) (left panel) and for the infinite-line problem (3.1) (right panel), with delay only in the inhibitor. The GM exponents are the prototypical set $(p, q, m, s) = (2, 1, 2, 0)$. In the left and right panels the boundaries of the shaded region are computed from the parametrization (2.36) and (3.26), respectively.

$(p, q, m, s) = (2, 1, 2, 0)$. We conclude that when T exceeds a threshold the spike solution is always unstable.

In §3 we analyze the linear stability of a one-spike steady-state for the 1-D infinite-line problem for (1.1) assuming that the delay only occurs in the inhibitor kinetics. For this case we set $D = 1$ and consider (1.1) on $-\infty < x < \infty$. For the parameter range $p = 2m-3$ with $m > 2$ where the NLEP is explicitly solvable, in §3.1 we analytically determine the Hopf bifurcation boundary in the τ versus T plane. For an arbitrary GM exponent set, in §3.2 we formulate and implement a simple numerical method to readily compute the Hopf bifurcation boundary from a parametrization of the NLEP. For the prototypical GM exponent set $(p, q, m, s) = (2, 1, 2, 0)$ this boundary and the region of linear stability is shown in the right panel of Fig. 1.1. In §3.3 we compare theoretical predictions for the region of stability of a one-spike solution on a finite domain with corresponding full numerical results. Under delayed inhibitor kinetics, we show numerically that large-scale oscillations of the spike amplitude occur just beyond the Hopf bifurcation boundary.

In §4 we study the linear stability of an M-spot solution, with $M \geq 2$, for the GM model with prototypical parameter set $(p, q, m, s) = (2, 1, 2, 0)$ in a 2-D bounded domain Ω with delayed inhibitor kinetics. In our analysis we consider the weak-coupling regime of [26] where the inhibitor diffusivity D satisfies $D = \mathcal{O}(-\log \epsilon)$. In the absence of delay, it is well-known (cf. [26]) that the multi-spot pattern can be destabilized by either a synchronous perturbation of the spot amplitudes or by $M-1$ possible asynchronous perturbations of the spot amplitudes. By using a hybrid analytical-numerical approach to analyze the corresponding NLEP for either the synchronous or asynchronous modes, we determine phase diagrams in the three-dimensional parameter space τ, T, and $\mu = 2\pi M D_0/|\Omega|$, where the multi-spot pattern is linearly stable. Here $D = D_0/\nu$ with $\nu \equiv -1/\log \epsilon$ and $|\Omega|$ is the area of Ω.

In §5 we consider various limiting forms of the 1-D and 2-D GM model where we now assume that the reaction-kinetics have a time delay in both the activator and the inhibitor. We first formulate a generalized NLEP to encompass the infinite-line problem, the shadow problem, and the multi-spot problem in 2-D. Although it is intractable analytically to determine Hopf bifurcation boundaries from this NLEP, we provide a rigorous argument, based on continuity of paths of spectra, to prove that there is a critical value of the delay T at which a Hopf bifurcation occurs. Our numerical computations of the Hopf bifurcation boundary for the 1-D problem show that the phase diagram in the τ versus T plane is qualitatively very similar to the phase diagram that occurs when there is a time-delay only in the inhibitor kinetics.

Finally, in §6 we briefly summarize our main results and suggest a few open problems for further investigation.

2. Delay Effects: The Limiting Shadow Problem. In this section, we will analyze the shadow limit $D \to +\infty$ for the GM model (1.1). In the limit $D \to \infty$, (1.1) reduces to the so-called shadow problem for $v(x,t)$ and $u(t)$ (cf. [10])

$$v_t = \varepsilon^2 v_{xx} - v + v_T^p/u_T^q\,, \quad -1 < x < 1\,, \quad v_x(\pm 1,t) = 0\,; \qquad \tau u_t = -u + \frac{1}{2\varepsilon}\int_{-1}^{1} \frac{v_T^m}{u_T^s}\,dx\,. \tag{2.1}$$

For $\varepsilon \to 0$, a one-spike steady-state solution v_e, u_e for (2.1), with spike centered at $x = 0$, is given for $p > 1$ by (cf. [10])

$$v_e \sim U_e^{\gamma} w\,(x/\varepsilon)\;; \qquad U_e \sim \left(\frac{1}{2}\int_{-\infty}^{\infty} w^m\,dy\right)^{-1/\xi}\,, \qquad w = \left(\frac{p+1}{2}\right)^{1/(p-1)} \left(\operatorname{sech}\left(\frac{(p-1)}{2}y\right)\right)^{2/(p-1)}\,, \tag{2.2}$$

where $\gamma \equiv q/(p-1)$, and $w(y)$ is the unique positive homoclinic solution to

$$w'' - w + w^p = 0\,, \qquad -\infty < y < \infty\,; \qquad w \to 0 \quad \text{as} \quad |y| \to \infty\,; \qquad w'(0) = 0\,, \qquad w(0) > 0\,. \tag{2.3}$$

To study the stability of this steady-state solution we linearize (2.1) about (2.2) by introducing $v = v_e + e^{\lambda t}\Phi(x/\varepsilon)$, and $u = u_e + e^{\lambda t}\eta$. After a short calculation, similar to that done in [10] and [22], but now accounting for the effect of delayed reaction-kinetics, we obtain the nonlocal eigenvalue problem (NLEP) for $\Phi(y)$, with $\Phi \to 0$ as $|y| \to \infty$, given by

$$L_T\Phi - \frac{mqe^{-2\lambda T}}{1+\tau\lambda+se^{-\lambda T}} w^p \frac{\int_{-\infty}^{\infty} w^{m-1}\Phi\,dy}{\int_{-\infty}^{\infty} w^m\,dy} = \lambda\Phi\,, \qquad -\infty < y < \infty\,; \qquad L_T\Phi \equiv \Phi'' - \Phi + pw^{p-1}e^{-\lambda T}\Phi\,. \tag{2.4}$$

For the simpler case where the delayed reaction-kinetics in (2.1) only arises in the inhibitor u and not in the activator v, so that $v_T = v$ in (2.1), the NLEP (2.4) is replaced by

$$L_0\Phi - \frac{mqe^{-\lambda T}}{1+\tau\lambda+se^{-\lambda T}} w^p \frac{\int_{-\infty}^{\infty} w^{m-1}\Phi\,dy}{\int_{-\infty}^{\infty} w^m\,dy} = \lambda\Phi\,, \qquad -\infty < y < \infty\,; \qquad L_0\Phi \equiv \Phi'' - \Phi + pw^{p-1}\Phi\,. \tag{2.5}$$

2.1. Inhibitor Delay: The Spectrum Near the Origin with Large Delay. For the NLEP (2.5) we now determine the spectrum near $\lambda = 0$ in the limit of large delay $T \gg 1$. We first write (2.5) as

$$L_0\Phi - \chi_s w^p \frac{\int_{-\infty}^{\infty} w^{m-1}\Phi\,dy}{\int_{-\infty}^{\infty} w^m\,dy} = \lambda\Phi\,, \qquad -\infty < y < \infty\,; \qquad \chi_s \equiv \frac{mq\mu}{1+\tau\lambda+s\mu}\,, \qquad \mu \equiv e^{-\lambda T}\,. \tag{2.6}$$

We let $T \to \infty$ and look for eigenvalues near the origin with $\lambda = \mathcal{O}(T^{-1})$. As a result of the identity $L_0 w = (p-1)w^p$, we obtain from (2.6) that $\lambda = 0$ when $\chi_s = (p-1)$. Upon writing $\lambda = c/T \ll 1$, so that $\mu = e^{-c}$, the condition $\chi_s = (p-1)$ determines c. In this way, we obtain the leading-order estimate for $T \gg 1$ that

$$\lambda \sim c/T\,, \qquad c \equiv \ln(1+\xi) + 2n\pi i\,, \tag{2.7}$$

where $n = 0, \pm 1, \pm 2, \ldots$, and $\xi > 0$ is defined in (1.1b) in terms of the GM exponents (p,q,m,s). Therefore, for a fixed large value of the delay, there are many eigenvalues near the origin in the unstable right half-plane $\operatorname{Re}(\lambda) > 0$.

To determine a more refined approximation for the eigenvalues of (2.6) near $\lambda = 0$, we substitute the expansion

$$\Phi = w + \Phi_1/T + \cdots\,, \qquad \lambda = c/T + c_1/T^2 + \cdots\,, \tag{2.8}$$

into (2.6), expand $\chi_s = (p-1) + \chi_{s1}/T + \ldots$, and collect terms of order $\mathcal{O}(T^{-1})$. This readily yields that

$$\mathcal{L}_0\Phi_1 \equiv L_0\Phi_1 - (p-1)w^p \frac{\int_{-\infty}^{\infty} w^{m-1}\Phi_1\,dy}{\int_{-\infty}^{\infty} w^m\,dy} = \chi_{s1} w^p + cw\,; \qquad \chi_{s1} \equiv -(p-1)\left(\frac{c_1 + \tau c}{1+se^{-c}}\right)\,. \tag{2.9}$$

Since $\mathcal{L}_0 w = 0$, the corresponding homogeneous adjoint problem

$$\mathcal{L}_0^\star \Psi_1 \equiv L_0 \Psi_1 - (p-1) w^{m-1} \frac{\int_{-\infty}^{\infty} w^p \Psi_1 \, dy}{\int_{-\infty}^{\infty} w^m \, dy} = 0 \,, \tag{2.10}$$

has a nontrivial solution $\Psi_1 = \Psi_1^\star$. As such, the solvability condition for (2.9) is that $\chi_{s1} \int_{-\infty}^{\infty} \Psi_1^\star w^p \, dy = -c \int_{-\infty}^{\infty} \Psi_1^\star w \, dy$. Upon using (2.9) for χ_{s1}, the expression above can be solved for c_1 as

$$c_1 = -\tau c + c \frac{(s+1+\xi)}{(1+\xi)(p-1)} \frac{I_1}{I_p} \,, \qquad \text{where} \qquad I_n \equiv \int_{-\infty}^{\infty} \Psi_1^\star w^n \, dy \,. \tag{2.11}$$

To calculate the integral ratio I_1/I_p in (2.11) we use the readily-derived identity $L_0^{-1} w = w/(p-1) + y w'/2$. We multiply (2.10) by $L_0^{-1} w$ and integrate by parts, using the decay of w as $y \to \pm\infty$, to obtain

$$\int_{-\infty}^{\infty} \left(L_0^{-1} w \right) \left(L_0 \Psi_1^\star \right) \, dy = I_1 = \frac{(p-1) I_p}{\int_{-\infty}^{\infty} w^m \, dy} \int_{-\infty}^{\infty} w^{m-1} \left(L_0^{-1} w \right) dy \,.$$

Then, upon using our expression for $L_0^{-1} w$, we obtain that

$$\frac{I_1}{I_p} = \frac{(p-1)}{\int_{-\infty}^{\infty} w^m \, dy} \int_{-\infty}^{\infty} \left(\frac{w^m}{p-1} + \frac{1}{2} y w^{m-1} w' \right) dy = 1 + \frac{(p-1)}{2m} \frac{\int_{-\infty}^{\infty} y \left(w^m \right)' \, dy}{\int_{-\infty}^{\infty} w^m \, dy} \,.$$

Finally, upon integrating by parts, we get $I_1/I_p = 1 - (p-1)/(2m)$, which determines c_1 from (2.11). From (2.8), this yields a two-term expansion for λ in the limit of large delay $T \gg 1$,

$$\lambda \sim \frac{c}{T} \left(1 + \frac{f}{T} + \cdots \right) \,, \qquad f = -\tau + \frac{mq}{(p-1)^2 (1+\xi)} \left(1 - \frac{(p-1)}{2m} \right) \,; \qquad c \equiv \ln(1+\xi) + 2n\pi i \,. \tag{2.12}$$

For $m = 2$ and $1 < p \leq 5$, and with no delay $T = 0$, we recall from Theorem 2.3 of [22] that there is a unique critical Hopf bifurcation value $\tau = \tau_H^0 > 0$ for which (2.5) has a complex conjugate pair of eigenvalues $\lambda = \pm i \lambda_{IH}^0$ with $\lambda_{IH}^0 > 0$, with $\mathrm{Re}(\lambda) > 0$ for $\tau > \tau_H^0$ and $\mathrm{Re}(\lambda) < 0$ for $\tau < \tau_H^0$. Since (2.12) shows that there are eigenvalues in $\mathrm{Re}(\lambda) > 0$ for large delay $T \gg 1$, this suggests that there should be a sequence of Hopf bifurcations at some critical values of the delay T for any $\tau < \tau_H^0$. This issue is explored in detail below for a special subrange of the GM exponents.

2.2. Inhibitor Delay Effects: An Explicitly Solvable NLEP. We now show that under certain conditions on the exponents m and p the determination of the point spectrum of (2.5) in the right half-plane $\mathrm{Re}(\lambda) > 0$ can be reduced to the study of a rather simple transcendental equation in λ. As such, for this subrange of exponents the effect of delayed inhibitor reaction-kinetics is readily analyzed. We first recall some properties of the local eigenvalue problem $L_0 \phi_l = \nu \phi_l$ on $\mathbb{R}$ for $\phi_l \in \mathcal{H}^1(\mathbb{R})$. From [16], this problem admits the eigenvalues $\nu_0 > 0$ and $\nu_1 = 0$, where ν_0 is simple, and the corresponding eigenfunction ϕ_{l0} has one sign. Furthermore, from Proposition 5.6 of [4], when $p \geq 3$ there are no discrete eigenvalues for L_0 in the interval $(-1, 0)$. The continuous spectrum for L_0 is the segment $\lambda < -1$ with λ real.

As shown in Lemma 2.3 of [19], when $p = 2m - 3$ and $m > 2$, we have the key identity that

$$L_0 \left(w^{m-1} \right) = (m^2 - 2m)(w^{m-1}) \,. \tag{2.13}$$

We now use this identity to characterize the unstable point spectrum of the NLEP (2.5) for a particular parameter range.

Lemma 2.1. *Consider the NLEP (2.5) when $p = 2m - 3$ and $m > 2$, corresponding to eigenfunctions for which $\int_{-\infty}^{\infty} w^{m-1} \Phi \, dy \neq 0$. Then, any unstable eigenvalues in $Re(\lambda) > 0$ for (2.5) must satisfy the transcendental equation*

$$\lambda = (m^2 - 2m) - \frac{m}{2} \chi_s \,, \qquad \chi_s \equiv \frac{mq\mu}{1 + \tau\lambda + s\mu} \,, \qquad \mu \equiv e^{-\lambda T} \,. \tag{2.14}$$

The remaining eigenfunctions Φ, for which $\int_{-\infty}^{\infty} w^{m-1} \Phi \, dy = 0$, are simply the eigenfunctions of L_0 corresponding to the zero eigenvalue and any negative real eigenvalues.

Proof. We use Green's identity on w^{m-1} and Φ, together with the far-field decay for Φ and w as $|y| \to \infty$, to get $\int_{-\infty}^{\infty} \left(w^{m-1} L_0 \Phi - \Phi L_0 w^{m-1} \right) dy = 0$. Then, substituting $L_0\Phi$ from (2.5) and $L_0 w^{m-1} = (m^2 - 2m) w^{m-1}$, we get

$$\left(\int_{-\infty}^{\infty} w^{m-1} \Phi \, dy \right) \left(\lambda - (m^2 - 2m) + \chi_s \frac{\int_{-\infty}^{\infty} w^{3m-4} \, dy}{\int_{-\infty}^{\infty} w^m \, dy} \right) = 0 \, .$$

For eigenfunctions for which $\int_{-\infty}^{\infty} w^{m-1} \Phi \, dy \neq 0$, the first factor is non-vanishing, and we conclude

$$\lambda = m^2 - 2m - \chi_s \frac{\int_{-\infty}^{\infty} w^{3m-4} \, dy}{\int_{-\infty}^{\infty} w^m \, dy} \, . \tag{2.15}$$

To calculate the integral ratio in (2.15), we multiply $w'' - w + w^{2m-3} = 0$ by w^{m-1} and we multiply the identity $L_0 w^{m-1} = (m^2 - 2m) w^{m-1}$ by w. We subtract the resulting two expressions and integrate over $-\infty < y < \infty$. Upon using $w \to 0$ as $|y| \to \infty$ we obtain that $(2m-4) \int_{-\infty}^{\infty} w^{3m-4} \, dy = (m^2 - 2m) \int_{-\infty}^{\infty} w^m \, dy$. Therefore, the integral ratio in (2.15) is $\int_{-\infty}^{\infty} w^{3m-4} \, dy = \left(\int_{-\infty}^{\infty} w^m \, dy \right) (m/2)$, which yields (2.14).

Next, consider the eigenfunctions for which $\int_{-\infty}^{\infty} w^{m-1} \Phi \, dy = 0$. From (2.13), together with the facts that w^{m-1} is the unique and one-signed principal eigenfunction of L_0, and that any eigenfunctions of the self-adjoint operator L_0 must be orthogonal, it follows that these other eigenfunctions must belong to the set of eigenfunctions of L_0 corresponding to the zero eigenvalue and any negative real eigenvalues of L_0. □

We now study the roots of (2.14) in $\mathrm{Re}(\lambda) \geq 0$, after first writing (2.14) as

$$(1 + \tau\lambda) e^{\lambda T} = -s + \frac{m^2 q}{2 \left(\beta - \lambda \right)} \, , \qquad \beta \equiv m^2 - 2m \, . \tag{2.16}$$

With no delay, so that $T = 0$, (2.16) reduces to the quadratic equation

$$\lambda^2 - \left(\beta - \frac{(1+s)}{\tau} \right) \lambda + \frac{\beta \xi}{\tau} = 0 \, , \qquad \xi \equiv \frac{mq}{2m-4} - (s+1) \, . \tag{2.17}$$

Since $p = 2m - 3$, the condition (1.1b) on the GM exponents yields $\xi > 0$. From (2.17) we conclude that there is a unique Hopf bifurcation value $\tau = \tau_H^0$, with $\lambda = i\lambda_{IH}^0$, for which $\mathrm{Re}(\lambda) < 0$ if $\tau < \tau_H^0$ and $\mathrm{Re}(\lambda) > 0$ if $\tau > \tau_H^0$, given by

$$\tau_H^0 = \frac{(1+s)}{\beta} \, , \qquad \lambda_{IH}^0 = \frac{\beta \sqrt{\xi}}{\sqrt{1+s}} \, . \tag{2.18}$$

Next, we show that if $0 < s < 1$, there is a minimal positive value of the delay T for which (2.16) has a purely imaginary complex conjugate pair of roots when $\tau = 0$. To show this, we set $\tau = 0$ and $\lambda = i\lambda_{IH}$ in (2.16). Upon separating the real and imaginary parts of the resulting expression we obtain

$$\cos\left(\lambda_{IH} T \right) = -s + \frac{m^2 q \beta}{2(\beta^2 + \lambda_{IH}^2)} \, , \qquad \sin\left(\lambda_{IH} T \right) = \frac{m^2 q \lambda_{IH}}{2(\beta^2 + \lambda_{IH}^2)} \, . \tag{2.19}$$

We square both sides of this expression and add, and after introducing $\xi = m^2 q/(2\beta) - (s+1)$, we derive that

$$\Big| -s + \frac{m^2 q}{2(\beta - i\lambda_{IH})} \Big|^2 = \frac{1}{\beta^2 + \lambda_{IH}^2} \left(\left(\frac{m^2 q}{2} \right)^2 - m^2 q \beta s \right) + s^2 = \frac{\beta^2 \left(\xi + 1 \right)^2 + s^2 \lambda_{IH}^2}{\beta^2 + \lambda_{IH}^2} = 1 \, . \tag{2.20}$$

Since $\xi > 0$, and assuming that $0 < s < 1$, we obtain that $\lambda_{IH} = \lambda_{IH}^{\mathrm{f}}$, where

$$\lambda_{IH}^{\mathrm{f}} \equiv \frac{\beta}{\sqrt{1 - s^2}} \left[\left(\xi + 1 \right)^2 - 1 \right]^{1/2} \, , \qquad \text{where} \qquad \beta = m^2 - 2m \, , \qquad \xi \equiv \frac{mq}{2m-4} - (1+s) \, . \tag{2.21}$$

Then, to determine the minimum critical value of the delay T, we substitute (2.21) into (2.19), to obtain

$$\sin\left(\lambda_{IH}^{\rm f} T\right) = \frac{m^2 q}{2\beta}(1-s^2)^{1/2}\frac{\left[(\xi+1)^2-1\right]^{1/2}}{(\xi+1)^2-s^2}\,.$$

We then use $m^2q/(2\beta) = \xi + (s+1)$ in this expression, to obtain that $T = T^{\rm f}$, where

$$T^{\rm f} \equiv \frac{1}{\lambda_{IH}^{\rm f}}\sin^{-1}\left((1-s^2)^{1/2}\frac{\left[(\xi+1)^2-1\right]^{1/2}}{(\xi+1)-s}\right)\,. \tag{2.22}$$

Therefore, if $0 < s < 1$, we conclude that there is a Hopf bifurcation value T^f of T even when $\tau = 0$. We remark that further Hopf bifurcations occur at the larger values of the delay $T_n^{\rm f} = T^{\rm f} + 2\pi n/\lambda_{IH}$ for $n \geq 1$, where n is an integer. For the exponent set $(p,q,m,s) = (3,2,3,0)$, for which $\beta = 3$ and $\xi = 2$, we get from (2.21) and (2.22) that

$$\lambda_{IH}^{\rm f} = 6\sqrt{2}\,, \qquad T^{\rm f} = \frac{1}{6\sqrt{2}}\sin^{-1}\left(\frac{2\sqrt{2}}{3}\right) \approx 0.145\,. \tag{2.23}$$

Next, we seek a parametrization in the τ versus T plane, corresponding to the minimal value of T for which a Hopf bifurcation occurs. To do so, we write (2.16) in the form

$$e^{\lambda T} = \frac{1}{1+\tau\lambda}\left(-s + \frac{m^2 q}{2\,(\beta-\lambda)}\right)\,. \tag{2.24}$$

We let $\lambda = i\lambda_{IH}$ with $\lambda_{IH} = \omega_0\beta$, and set the modulus of (2.24) to unity. Upon using (2.20), we get

$$\tau^2\beta^2\omega_0^2 + 1 = \frac{(\xi+1)^2 + s^2\omega_0^2}{\omega_0^2+1}\,.$$

Upon solving for τ, and then taking the imaginary part of (2.24), we obtain the following parameteric description, in terms of ω_0, of the curve in the τ versus T plane where the minimal Hopf bifurcation occurs:

$$\tau = \frac{1}{\beta\omega_0}\sqrt{\frac{(\xi+1)^2 - 1 + (s^2-1)\omega_0^2}{1+\omega_0^2}}\,, \qquad T = \frac{1}{\omega_0\beta}\sin^{-1}\left(\frac{\omega_0\left[(1+\xi+s) - \tau\beta(1+\xi-s\omega_0^2)\right]}{(\xi+1)^2+\omega_0^2 s^2}\right)\,, \tag{2.25}$$

where $\beta = m^2 - 2m$. The corresponding eigenvalue is $\lambda = i\omega_0\beta$. For $0 < s < 1$, we require that $\sqrt{\xi/(s+1)} < \omega_0 < \sqrt{\left[(\xi+1)^2-1\right]/(1-s^2)}$, where the lower limit for ω_0 corresponds to $T = 0$, and the upper limit is where $\tau = 0$.

Alternatively, for $s \geq 1$, we need only that $\omega_0 > \left(\xi/(s+1)\right)^{1/2}$ in (2.25), and so on the Hopf bifurcation boundary we must have $\tau > 0$. By taking the limit $\omega_0 \to +\infty$ in (2.25), and recalling that $\lambda_{IH} = \beta\omega_0$, we derive for $\tau \to 0^+$ that

$$T \sim \frac{\tau}{\sqrt{s^2-1}}\sin^{-1}\left(\frac{\sqrt{s^2-1}}{s}\right)\,, \qquad \lambda_{IH} \sim \frac{\sqrt{s^2-1}}{\tau}\,, \qquad s > 1\,, \tag{2.26a}$$

$$T \sim \left(1 + \sqrt{\frac{\xi+2}{\xi}}\right)\tau\,, \qquad \lambda_{IH} \sim \sqrt{\frac{\beta}{\tau}}\left(\xi^2+2\xi\right)^{1/4}\,, \qquad s = 1\,. \tag{2.26b}$$

We remark that the limiting expression (2.26a) is not uniformly valid as $s \to 1^+$.

We now illustrate our results. For the special case $(p,q,m,s) = (3,2,3,0)$, for which $\xi = 2$ and $\beta = 3$, (2.25) becomes

$$\tau = \frac{1}{3\omega_0}\sqrt{\frac{8-\omega_0^2}{1+\omega_0^2}}\,, \qquad T = \frac{1}{3\omega_0}\sin^{-1}\left(\frac{\omega_0}{3}(1-3\tau)\right)\,. \tag{2.27}$$

For this parameter set, the stability boundary (2.27) is shown in the left panel of Fig. 2.1. For the qualitatively different case where $(p,q,m,s) = (3,2,3,1)$, for which $s = 1$, there is no longer any Hopf bifurcation value of $T > 0$ when $\tau = 0$.

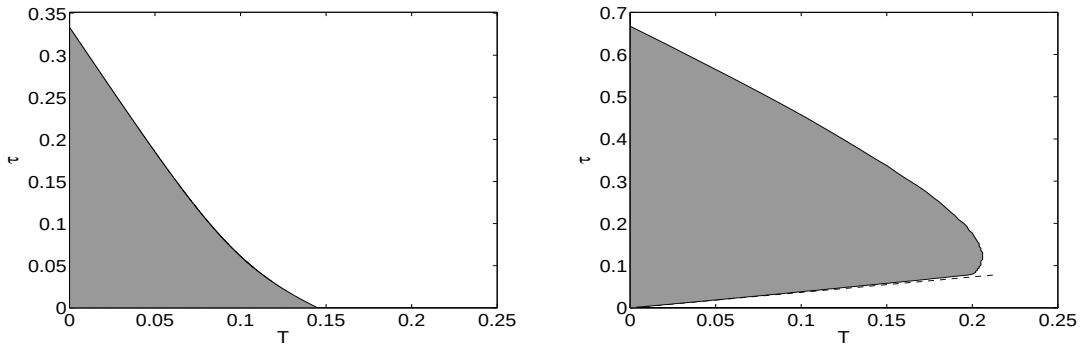

Fig. 2.1: The stable shaded region in the τ versus T plane for a one-spike solution to the shadow problem, with delay only in the inhibitor, as governed by the NLEP (2.5). Left: The exponent set $(p, q, m, s) = (3, 2, 3, 0)$. The boundary of the shaded region is given by (2.27). Right: $(p, q, m, s) = (3, 2, 3, 1)$. The boundary of the shaded region is given by (2.25). Since $s = 1$, we do not have a Hopf bifurcation at some $T > 0$ when $\tau = 0$. The dashed line is the limiting approximation given in (2.26b), valid for $\tau \to 0^+$, which agrees closely with the numerically computed Hopf bifurcation boundary.

For $\omega_0 \gg 1$, we have from (2.26b) that the stability boundary satisfies $\tau \to 0$ and $T \to 0$ as $\omega_0 \to \infty$. A plot of the stability boundary in the τ versus T plane, as computed from (2.25), is shown in the right panel of Fig. 2.1 together with the limiting approximation given in (2.26b), which is valid for $\tau \to 0^+$. This limiting approximation is seen to provide a very accurate determination of the lower stability boundary.

In the left panel of Fig. 2.2 we show the other Hopf bifurcations that occur for the larger values of T given by $T_n = T + 2\pi n/(3\omega_0)$ for $n \geq 1$, with n an integer, where T is given by (2.27). In the left panel of Fig. 2.2, we also show the curve in the τ versus T plane where real roots of (2.16) first occur. We further remark that the large T asymptotics of (2.16), as obtained by substituting $\lambda = c/T + c_1/T^2 + \cdots$ into (2.16), agrees with the general result (2.12) when $p = 2m - 3$. For the special case where $(p, q, m, s) = (3, 2, 3, 0)$, (2.12) reduces to

$$\lambda \sim \frac{c}{T}\left(1 + \frac{1}{T}\left(\frac{1}{3} - \tau\right) + \cdots\right), \qquad c = \ln 3 + 2n\pi i\,, \quad n = 0, \pm 1, \pm 2, \ldots\,. \tag{2.28}$$

In the right panel of Fig. 2.2, this two-term expansion for large T is favorably compared with corresponding results, computed numerically from (2.16), for $\tau = 0.2$ and $(p, q, m, s) = (3, 2, 3, 0)$.

In summary, these results show that a time-delay in the inhibitor concentration destabilizes the spike solution for the shadow problem in the sense that there exists a critical value $T_{\min}$ of T for which the spike is unstable for all $\tau \geq 0$ when $T > T_{\min}$. Although we have only given an analysis of this for GM exponent sets where the NLEP is explicitly solvable, the numerical computations shown in Fig. 1.1 for the standard exponent set $(p, q, m, s) = (2, 1, 2, 0)$ reveals a similar behavior. In the next section, we show how the Hopf bifurcation boundary is readily computed numerically for arbitrary GM exponents sets for the 1-D or 2-D shadow problem.

2.3. Inhibitor Delay: The Shadow Problem in 2-D. Next, we consider the following shadow problem in an N-dimensional bounded domain Ω, where $N = 1, 2$, assuming only a delayed reaction-kinetics in the inhibitor:

$$v_t = \varepsilon^2 \Delta v - v + v^p/u_T^q\,, \quad x \in \Omega\,, \qquad \partial_n v = 0\,, \quad x \in \partial\Omega\,; \qquad \tau u_t = -u + \frac{1}{|\Omega|}\int_\Omega \frac{v^m}{u_T^s}\,dx\,, \tag{2.29}$$

where $|\Omega|$ denotes the measure of Ω. A one-spike steady-state solution to (2.29) is given by (cf. [24], [10], [22])

$$v_e \sim U_e^\gamma w\left[\varepsilon^{-1}|x - x_0|\right], \qquad U_e \sim \left(\frac{1}{|\Omega|}\int_{\mathbb{R}^2}\left[w\left(|y|\right)\right]^m\,dy\right)^{-1/\xi}, \tag{2.30}$$

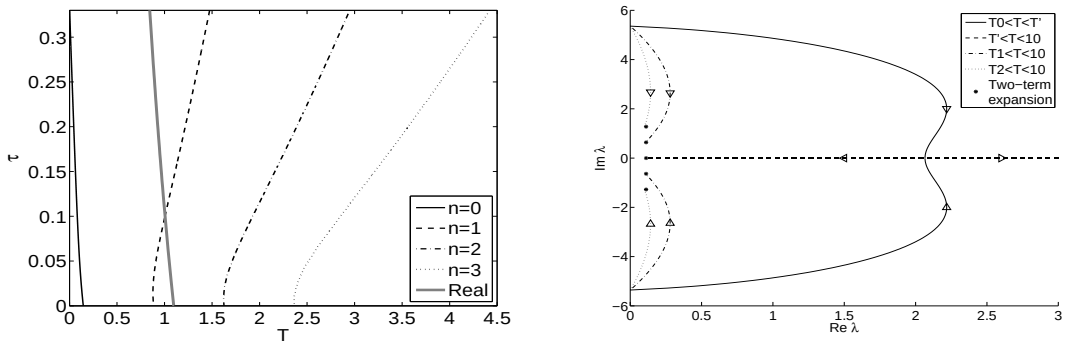

Fig. 2.2: The shadow problem (2.16) for the exponent set $(p, q, m, s) = (3, 2, 3, 0)$, with delay only in the inhibitor, characterized by the NLEP (2.5). Left: Hopf bifurcation curves (dashed curves) in the τ versus T plane for which additional complex conjugate pairs, indexed by n, enter the region $\mathrm{Re}(\lambda) > 0$. The thick line indicates when eigenvalues for (2.5) first appear as a double root on the positive real axis. Right panel: Paths of unstable eigenvalues versus T when $\tau = 0.2$. The heavy solid curve is the path associated with the primary Hopf bifurcation on the interval $T \in [T_0, T']$ where $T_0 \approx 0.578$ is the smallest Hopf bifurcation value of the delay, and $T' \approx 0.9292$ is the delay where a real eigenvalue appears. On the interval $T \in [T', 10]$ (dashed horizontal line) there are two real positive eigenvalues, with one tending to the origin as T increases (corresponding to $n = 0$ in (2.28)). The dashed-dotted and faint dotted curves are eigenvalue paths that emerge in the right half-plane through additional Hopf bifurcation points occurring at $T_1 \approx 1.2792$, and $T_2 \approx 2.4420$. The black dots near the origin are the two-term asymptotic result (2.28), valid for large delay, evaluated at $T = 10$ for $n = 0, 1, 2$.

for some $x_0 \in \Omega$, where $\gamma = q/(p-1)$ and ξ is defined in (1.1b). Here $y = \varepsilon^{-1}(x - x_0)$, where $w(\rho)$ with $\rho = |y|$ is the unique radially symmetric ground-state solution to the following BVP, in which $\Delta_\rho w \equiv w'' + (N-1)w'/\rho$:

$$\Delta_\rho w - w + w^p = 0\,, \quad 0 < \rho < \infty\,; \qquad w(0) > 0\,, \quad w'(0) = 0\,; \qquad w \to 0 \quad \text{as} \quad \rho \to \infty\,. \tag{2.31}$$

By proceeding similarly as in [22], but now allowing for delayed inhibitor kinetics, the NLEP governing the stability of the steady-state solution (2.30) is

$$L_0\Phi - \chi_s w^p \frac{\int_0^\infty \rho^{N-1} w^{m-1}\Phi\, d\rho}{\int_0^\infty \rho^{N-1} w^m\, d\rho} = \lambda\Phi\,, \qquad 0 < \rho < \infty\,; \qquad \chi_s(\lambda) \equiv \frac{mqe^{-\lambda T}}{1 + \tau\lambda + se^{-\lambda T}}\,, \tag{2.32}$$

where $\Phi = \Phi(\rho) \to 0$ as $\rho = |y| \to \infty$, and $L_0\Phi = \Delta_\rho\Phi - \Phi + pw^{p-1}\Phi$. It is readily shown (cf. [22]) that any unstable eigenvalue of (2.30) must be a root of $g(\lambda) = 0$, where

$$g(\lambda) = \frac{1}{\chi_s(\lambda)} - \mathcal{F}(\lambda)\,; \qquad \mathcal{F}(\lambda) \equiv \frac{\int_0^\infty \rho^{N-1} w^{m-1}\left[(L_0 - \lambda)^{-1} w^p\right]\, d\rho}{\int_0^\infty \rho^{N-1} w^m\, d\rho}\,. \tag{2.33}$$

We now seek a parametrization of the Hopf bifurcation boundary for (2.29) in the τ versus T plane. We let $\lambda = i\lambda_{IH}$ and set $g(i\lambda_{IH}) = 0$ in (2.33) to obtain

$$e^{i\lambda_{IH}T} = \frac{mq\mathcal{F}(i\lambda_{IH}) - s}{1 + i\tau\lambda_{IH}}\,, \qquad \text{where} \qquad \mathcal{F}(i\lambda_{IH}) = \mathcal{F}_R(\lambda_{IH}) + i\mathcal{F}_I(\lambda_{IH})\,. \tag{2.34a}$$

By separating $\mathcal{F}(i\lambda_{IH})$ into real and imaginary parts we get

$$\mathcal{F}_R(\lambda_{IH}) \equiv \frac{\int_0^\infty \rho^{N-1} w^{m-1} L_0\left[L_0^2 + \lambda_{IH}^2\right]^{-1} w^p\, d\rho}{\int_0^\infty \rho^{N-1} w^m\, d\rho}\,, \qquad \mathcal{F}_I(\lambda_{IH}) \equiv \frac{\lambda_{IH}\int_0^\infty \rho^{N-1} w^{m-1}\left[L_0^2 + \lambda_{IH}^2\right]^{-1} w^p\, d\rho}{\int_0^\infty \rho^{N-1} w^m\, d\rho}\,. \tag{2.34b}$$

By taking the modulus of both sides of (2.34a), and labeling $\mathcal{F}_R \equiv \mathcal{F}_R(\lambda_{IH})$ and $\mathcal{F}_I \equiv \mathcal{F}_I(\lambda_{IH})$, we obtain that

$$\tau^2 \lambda_{IH}^2 = \mathcal{N}_s(\lambda_{IH}) \equiv (mq\mathcal{F}_R - s)^2 + (mq\mathcal{F}_I)^2 - 1\,. \tag{2.35}$$

On the range of λ_{IH} for which $\mathcal{N}_s(\lambda_{IH}) > 0$, we can solve for τ, and then take the imaginary part of (2.34a) to obtain the following parametric representation of the Hopf bifurcation boundary in the τ versus T plane:

$$\tau \equiv \frac{1}{\lambda_{IH}}\sqrt{\mathcal{N}_s(\lambda_{IH})}\,, \qquad T \equiv \frac{1}{\lambda_{IH}}\sin^{-1}\left(\frac{-mq\tau\lambda_{IH}\mathcal{F}_R + s\tau\lambda_{IH} + mq\mathcal{F}_I}{1+\mathcal{N}_s(\lambda_{IH})}\right). \tag{2.36}$$

From this formulation it is easy to prove that when $s < 1$, that there is a Hopf bifurcation value T^f even when $\tau = 0$. To prove this we need only show that there is a root $\lambda_{IH} = \lambda_{IH}^f$ to $\mathcal{N}_s(\lambda_{IH}) = 0$. From [22] we have $\mathcal{F}_R(0) = 1/(p-1)$, $\mathcal{F}_I(0) = 0$, together with $\mathcal{F}_R(\lambda_I) = \mathcal{O}(\lambda_{IH}^{-2})$ and $\mathcal{F}_I(\lambda_I) = \mathcal{O}(\lambda_{IH}^{-1})$ as $\lambda_{IH} \to \infty$. In this way, since

$$\mathcal{N}_s(0) = (\xi+1)^2 - 1 > 0\,, \qquad \lim_{\lambda_{IH}\to\infty}\mathcal{N}_s(\lambda_{IH}) = s^2 - 1 < 0\,, \tag{2.37a}$$

it follows that $\mathcal{N}_s(\lambda_{IH}) = 0$ for some $\lambda_{IH} = \lambda_{IH}^f > 0$. Then, by using (2.36) for T, the Hopf bifurcation value is

$$T^f = \frac{1}{\lambda_{IH}}\sin^{-1}\left(mq\mathcal{F}_I(\lambda_{IH})\right)\,. \tag{2.37b}$$

This establishes for our general shadow problem that whenever $s < 1$ there must be a Hopf bifurcation value of the delay when $\tau = 0$ for any GM exponent set satisfying (1.1b) in either 1-D or 2-D.

We remark that if we take $p = 2m - 3$ for the 1-D problem where $N = 1$, for which the NLEP is explicitly solvable, we can readily calculate that $\mathcal{F}(\lambda) = m/[2(\beta - \lambda)]$ where $\beta = m^2 - 2m$. For this special case, a simple calculation shows that the parametrization (2.36) reduces to (2.25), while (2.37b) agrees with (2.22).

We now use the parametrization (2.36) to calculate Hopf bifurcation curves in the τ versus T plane for a few GM exponent sets. To compute $\mathcal{F}_R(\lambda_{IH})$ and $\mathcal{F}_I(\lambda_{IH})$ numerically we adopt the simple numerical procedure of [22] after first computing the ground-state solution w. With this numerical procedure, the Hopf bifurcation curve for the 1-D shadow problem for the prototypical GM exponent $(p, q, m, s) = (2, 1, 2, 0)$ is shown in Fig. 1.1. In the left panel of Fig. 2.3 we plot the Hopf bifurcation curve in the τ versus T parameter plane for the 2-D shadow problem for the parameter set $(p, q, m, s) = (3, 2, 3, 0)$, which was previously considered for the 1-D case in Fig. 2.1. With no delay, i.e. $T = 0$, there is a unique Hopf bifurcation value when $\tau \approx 0.182$, with corresponding eigenvalue $\lambda \approx 7.56i$. In the right panel of Fig. 2.3 we plot a similar Hopf bifurcation boundary when $(p, q, m, s) = (3, 2, 3, 1)$ for the 2-D shadow problem. In this latter case, where $s = 1$, we have $T \to 0$ as $\tau \to 0^+$, as was observed previously in Fig. 2.2 for the 1-D shadow problem.

Next, we analyze the spectrum of the NLEP (2.32) for large delay T. Since the identity $L_0 w = (p-1)w^p$ still holds in 2-D, we can proceed similarly as in (2.8)–(2.12) to determine the spectrum of the NLEP (2.32) for the 2-D shadow problem near the origin in the limit $T \gg 1$ of large delay. We set $N = 2$ and readily derive that

$$\lambda \sim \frac{c}{T}\left(1 + \frac{f}{T} + \cdots\right), \qquad f \equiv -\tau + \frac{mq}{(p-1)^2(\xi+1)}\frac{I_1}{I_p}\,, \qquad I_n \equiv \int_0^\infty \rho w^n \Psi_1^\star\, d\rho\,, \tag{2.38}$$

where $c = \ln(1+\xi) + 2n\pi i$, with $n = 0, \pm 1, \pm 2, \ldots$. Here $\Psi_1^\star(\rho)$ is the nontrivial solution of the adjoint problem

$$\mathcal{L}_0^\star \Psi_1 \equiv L_0\Psi_1 - (p-1)w^{m-1}\frac{\int_0^\infty w^p\Psi_1^\star\rho\, d\rho}{\int_0^\infty w^m\rho\, d\rho} = 0\,; \qquad \Psi_1^\star \to 0\,, \quad \text{as} \quad \rho\to\infty\,. \tag{2.39}$$

To calculate the integral ratio I_1/I_p in (2.38) we use the identity $L_0^{-1}w = w/(p-1) + \rho w'/2$ (cf. [22]), where $w(\rho)$ satisfies (2.31). We multiply (2.39) by $L_0^{-1}w$ and integrate by parts, using the decay of w as $\rho \to \pm\infty$, to obtain

$$\frac{I_1}{I_p} = \frac{(p-1)}{\int_0^\infty w^m\rho\, d\rho}\int_0^\infty \rho w^{m-1}\left(L_0^{-1}w\right)\, d\rho = \frac{(p-1)}{\int_0^\infty w^m\rho\, d\rho}\left[\frac{1}{p-1}\int_0^\infty w^m\rho\, d\rho + \frac{1}{2m}\int_0^\infty \rho^2\left(w^m\right)'\, d\rho\right].$$

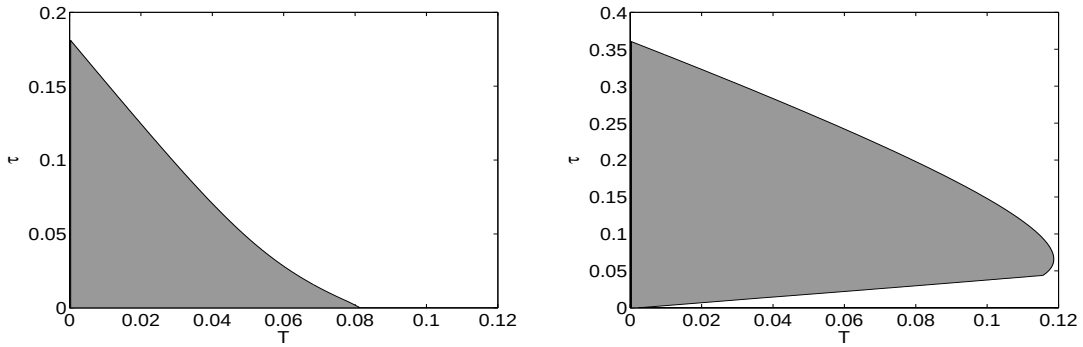

Fig. 2.3: Left: the stability region (shaded) in the τ versus T plane of the 2D shadow problem (2.29) with delayed inhibitor kinetics for the parameter set $(p, q, m, s) = (3, 2, 3, 0)$. Right: the corresponding stability region for the parameter set $(p, q, m, s) = (3, 2, 3, 1)$, where the Hopf bifurcation boundary satisfies $\tau \to 0$ as $T \to 0$.

Upon integrating the last expression by parts we get $I_1/I_p = 1 - (p-1)/m$. By combining this relation with (2.38), we obtain the following two-term expression for the eigenvalues near the origin in the limit $T \gg 1$ of large delay:

$$\lambda \sim \frac{c}{T}\left(1 + \frac{f}{T} + \cdots\right), \qquad f = -\tau + \frac{mq}{(p-1)^2(\xi+1)}\left(1 - \frac{(p-1)}{m}\right). \tag{2.40}$$

Here $c = \ln(1+\xi) + 2n\pi i$, with $n = 0, \pm 1, \pm 2, \ldots$. Apart from a factor of 2, this expression is identical to that derived in (2.12) for the 1-D problem, and shows that many eigenvalues cluster near the origin in the limit of large delay.

3. Delay Effects: An Explicitly Solvable NLEP Problem on the Infinite Line. In this section we analyze the stability of a one-spike solution to the following non-dimensionalized GM system with delayed reaction-kinetics:

$$v_t = \varepsilon^2 v_{xx} - v + v_T^p/u_T^q\,, \qquad \tau u_t = u_{xx} - u + \epsilon^{-1} v_T^m/u_T^s\,, \qquad -\infty < x < \infty\,, \quad t > 0\,, \tag{3.1}$$

where $u_T \equiv u(x, t-T)$ and $v_T = v(x, t-T)$, under the condition (1.1b) on the GM exponents (p, q, m, s). Since we are considering the infinite-line problem, without loss of generality we have specified a unit inhibitor diffusivity.

In [11] a one-spike steady-state solution to (3.1) was constructed for $\varepsilon \to 0$. The result is summarized as follows:

Principal Result 3.1. *For $\varepsilon \to 0$, a one-spike steady-state solution to (3.1), labeled by $v_e(x)$ and $u_e(x)$, is given by*

$$v_e(x) \sim U_0^{\gamma} w\left(\varepsilon^{-1} x\right); \qquad u_e(x) \sim U_0 \frac{G_0(x)}{G_0(0)}; \qquad U_0 = \left(\frac{1}{2}\int_{-\infty}^{\infty} w^m\, dy\right)^{-1/\xi}, \tag{3.2}$$

where $w(y)$ is the homoclinic satisfying (2.3), and where the Green's function $G_0(x) = e^{-|x|}/2$ in (3.2) satisfies $G_{0xx} - G_0 = -\delta(x)$ with $G_0 \to 0$ as $|x| \to \infty$. Here ξ is defined in (1.1b).

Next, we linearize (3.1) around the steady-state solution by introducing $v = v_e + e^{\lambda t}\phi$ and $u = u_e + e^{\lambda t}\eta$ where $\phi \ll 1$ and $\eta \ll 1$ in (3.1). This yields a singularly perturbed eigenvalue problem for $\phi(x)$ and $\eta(x)$ given by

$$\varepsilon^2 \phi_{xx} - \phi + \frac{p v_e^{p-1}}{u_e^q} e^{-\lambda T}\phi - \frac{q v_e^p}{u_e^{q+1}} e^{-\lambda T}\eta = \lambda\phi\,, \qquad -\infty < x < \infty\,, \tag{3.3a}$$

$$\eta_{xx} - (1 + \tau\lambda)\,\eta = -m\varepsilon^{-1}\frac{v_e^{m-1}}{u_e^s} e^{-\lambda T}\phi + s\varepsilon^{-1}\frac{v_e^m}{u_e^{s+1}} e^{-\lambda T}\eta\,, \qquad -\infty < x < \infty\,. \tag{3.3b}$$

In the limit $\varepsilon \to 0$, (3.3) can be reduced to a nonlocal eigenvalue problem (NLEP). Since a similar calculation was done in [11] for the case of no delay, we only briefly highlight the analysis here.

Since v_e is concentrated near $x=0$, we look for a localized eigenfunction for $\phi(x)$ in the form $\phi=\Phi\left(\varepsilon^{-1}x\right)$. Upon using $v_e\sim U_0^{\gamma}w$ and $u_e\sim U_0$ near $x=0$ from (3.2), where $\gamma=q/(p-1)$, we obtain from (3.3a) that $\Phi(y)$ satisfies

$$L_T\Phi - qU_0^{\gamma p-(q+1)}e^{-\lambda T}w^p\eta(0)=\lambda\Phi\,,\qquad -\infty<y<\infty\,;\qquad L_T\Phi\equiv\Phi''-\Phi+pw^{p-1}e^{-\lambda T}\Phi\,. \tag{3.4}$$

To derive the NLEP for $\Phi(y)$, we must determine $\eta(0)$ from (3.3b). Since $v_e\phi$ is concentrated only near $x=0$, we calculate for $\epsilon\to 0$ in the sense of distributions that

$$\begin{aligned} m\varepsilon^{-1}\frac{v_e^{m-1}}{u_e^s}e^{-\lambda T}\phi \quad &\to \quad mU_0^{\gamma(m-1)-s}e^{-\lambda T}\left(\int_{-\infty}^{\infty}w^{m-1}\Phi\,dy\right)\delta(x)\,,\\ s\varepsilon^{-1}\frac{v_e^{m}}{u_e^{s+1}}e^{-\lambda T}\eta \quad &\to \quad sU_0^{\gamma m-(s+1)}e^{-\lambda T}\eta(0)\left(\int_{-\infty}^{\infty}w^{m}\,dy\right)\delta(x)\,. \end{aligned}$$

Therefore, by using these relations in (3.3b), together with (3.2) for U_0, we obtain in the outer region $|x|\gg\mathcal{O}(\epsilon)$ that

$$\eta_{xx}-(1+\tau\lambda)\,\eta=-mU_0^{\gamma(m-1)-s}e^{-\lambda T}\left(\int_{-\infty}^{\infty}w^{m-1}\Phi\,dy\right)\delta(x)+2se^{-\lambda T}\eta(0)\,\delta(x)\,, \tag{3.5}$$

with $\eta\to 0$ as $|x|\to\infty$. To solve (3.5), we introduce the eigenvalue-dependent Green's function $G_\lambda(x)$ satisfying

$$G_{\lambda xx}-(1+\tau\lambda)G_\lambda=-\delta(x)\,,\quad -\infty<x<\infty\,;\qquad G_\lambda\to 0\quad\text{as}\quad |x|\to\infty\,. \tag{3.6}$$

The solution to (3.6) is simply $G_\lambda(x)=e^{-2\sqrt{1+\tau\lambda}|x|}/\left[2\sqrt{1+\tau\lambda}\right]$, where we must choose the principal branch of $\sqrt{1+\tau\lambda}$ to ensure that $G_\lambda\to 0$ as $|x|\to\infty$ for any λ with $\mathrm{Re}(\lambda)>0$.

We represent the solution to (3.5) in terms of G_λ, and in so doing we determine $\eta(0)$ as

$$\eta(0)=\left(\frac{m}{2}\right)\frac{U_0^{\gamma(m-1)-s}e^{-\lambda T}}{\sqrt{1+\tau\lambda}+se^{-\lambda T}}\int_{-\infty}^{\infty}w^{m-1}\Phi\,dy\,. \tag{3.7}$$

Upon substituting (3.7) into (3.4), we obtain the following NLEP for the case where both the activator and inhibitor have delayed reaction-kinetics:

$$L_T\Phi-\frac{mqe^{-2\lambda T}}{\sqrt{1+\tau\lambda}+se^{-\lambda T}}w^p\frac{\int_{-\infty}^{\infty}w^{m-1}\Phi\,dy}{\int_{-\infty}^{\infty}w^m\,dy}=\lambda\Phi\,,\qquad -\infty<y<\infty\,, \tag{3.8}$$

where $\Phi\to 0$ as $|y|\to\infty$. For the simpler case where the delayed reaction-kinetics in (3.1) only arises in the inhibitor u and not in the activator v, so that $v_T=v$ in (3.1), the NLEP (3.8) is replaced by

$$L_0\Phi-\frac{mqe^{-\lambda T}}{\sqrt{1+\tau\lambda}+se^{-\lambda T}}w^p\frac{\int_{-\infty}^{\infty}w^{m-1}\Phi\,dy}{\int_{-\infty}^{\infty}w^m\,dy}=\lambda\Phi\,,\qquad -\infty<y<\infty\,;\qquad L_0\Phi\equiv\Phi''-\Phi+pw^{p-1}\Phi\,. \tag{3.9}$$

3.1. Inhibitor Delay Effects: An Explicitly Solvable NLEP. In this subsection we analyze the spectrum of the NLEP (3.9) for the explicitly solvable case where $p=2m-3$ and $m>2$. By using Lemma 2.1 we obtain that any discrete eigenvalue of the NLEP (3.9) must be a root of

$$\sqrt{1+\tau\lambda}\,e^{\lambda T}=-s+\frac{m^2q}{2(\beta-\lambda)}\,,\qquad \beta=m^2-2m\,. \tag{3.10}$$

For the case of no delay, where $T=0$, it was shown in Principal Result 3.8 of [19] that there is a unique Hopf bifurcation value τ_H^0, with corresponding eigenvalue $\lambda=i\lambda_{IH}^0$, given by

$$\tau_H^0=\frac{(m^2q)^2}{2\zeta^2}\left(\beta-\frac{2s}{m^2q}\right)\,,\qquad \lambda_{IH}^0=\sqrt{\zeta-\beta^2}\,, \tag{3.11a}$$

where $\zeta > \beta^2$ is the smallest root of the quadratic

$$4(s^2-1)\zeta^2 - \left[(m^2q)^2 + 4\beta s(m^2q)\right]\zeta + 2\beta^2(m^2q)^2 = 0\,. \tag{3.11b}$$

For the exponent set $(p,q,m,s) = (3,2,3,1)$, we have $\tau_H^0 = 2.5$ and $\lambda_{IH}^0 = 3/\sqrt{5} \approx 1.34$. For $(p,q,m,s) = (3,2,3,0)$ we have $\tau_H^0 = [13+3\sqrt{17}]/12 \approx 2.114$ and $\lambda_{IH}^0 \approx 3\sqrt{3\sqrt{17}-11}/\sqrt{2} \approx 2.482$.

First, we determine whether there is a Hopf bifurcation value of T even when $\tau = 0$. By setting $\tau = 0$ in (3.10) we obtain the same problem considered in §2.2 for the shadow problem. Therefore, for $s < 1$ the Hopf bifurcation value T^f is given in (2.22) while the eigenvalue λ_{IH}^f is given in (2.21). For $s \geq 1$, there is no Hopf bifurcation when $\tau = 0$.

Next, we seek a parametrization of the Hopf bifurcation boundary in the τ versus T plane parameterized by $\lambda = i\lambda_{IH}$, where $\lambda_{IH} \equiv \beta\omega_0$. We first calculate that

$$\sqrt{1+i\tau\lambda_{IH}} = B_+ + iB_-\,, \qquad B_\pm \equiv \sqrt{\frac{\alpha \pm 1}{2}}\,, \qquad \alpha \equiv \sqrt{1+\tau^2\lambda_{IH}^2}\,. \tag{3.12}$$

Next, we isolate $e^{i\lambda_{IH}T}$ in (3.10) and take the modulus of the resulting expression. By using (2.20), we obtain that

$$\alpha = \Big| -s + \frac{m^2q}{2(\beta - i\lambda_{IH})}\Big|^2 = \frac{(\xi+1)^2 + s^2\omega_0^2}{1+\omega_0^2}\,. \tag{3.13}$$

Since $\alpha^2 = 1+\tau^2\beta^2\omega_0^2$, we can solve for $\tau = \tau(\omega_0)$ to obtain

$$\tau = \frac{\sqrt{\alpha^2-1}}{\beta\omega_0}\,, \qquad \alpha = \frac{(\xi+1)^2 + s^2\omega_0^2}{1+\omega_0^2}\,. \tag{3.14}$$

Next, to determine $T = T(\omega_0)$ we separate $e^{i\lambda_{IH}T}$ into real and imaginary parts after calculating that

$$e^{i\lambda_{IH}T} = \frac{(B_+ - iB_-)}{B_+^2 + B_-^2}\left(-s + \frac{m^2q\beta}{2(\beta^2+\lambda_{IH}^2)} + \frac{im^2q\lambda_{IH}}{2(\beta^2+\lambda_{IH}^2)}\right). \tag{3.15}$$

By using $m^2q/(2\beta) = \xi + s + 1$, $B_+^2 + B_-^2 = \alpha$, and writing $\lambda_{IH} = \beta\omega_0$, we derive from (3.15) that

$$T = \frac{1}{\beta\omega_0}\sin^{-1}\left[\frac{B_+\omega_0(\xi+s+1) + B_-(s\omega_0^2 - \xi - 1)}{\alpha(1+\omega_0^2)}\right], \tag{3.16}$$

where α is given in (3.14) and $B_\pm$ are defined in (3.12). In this way, (3.14) and (3.16) yields the Hopf bifurcation curve in the τ versus T plane, parameterized by ω_0. For $s < 1$, the range of ω_0 is $\lambda_{IH}^0/\beta < \omega_0 < \lambda_{IH}^f/\beta$, where λ_{IH}^0 and λ_{IH}^f are the Hopf eigenvalues for the limiting cases $T = 0$ and $\tau = 0$, as given in (3.11) and (2.21), respectively.

Alternatively, for $s \geq 1$, we need only that $\omega_0 > \lambda_{IH}^0/\beta$. By letting $\omega_0 \to \infty$ in (3.14) and (3.16) it is easy to show that the Hopf bifurcation boundary tends to the origin $(T,\tau) = (0,0)$ as $\omega_0 \to \infty$. In analogy with (2.26) we get

$$T \sim \frac{\tau}{\sqrt{s^4-1}}\sin^{-1}\left(\frac{\sqrt{s^2-1}}{\sqrt{2}s}\right), \qquad \lambda_{IH} \sim \frac{\sqrt{s^4-1}}{\tau}\,, \qquad s > 1\,, \tag{3.17a}$$

$$T \sim \left(1 + \sqrt{\frac{2\xi+4}{\xi}}\right)\frac{\tau}{2}\,, \qquad \lambda_{IH} \sim \sqrt{\frac{\beta}{\tau}}\left(2\xi^2+4\xi\right)^{1/4}\,, \qquad s = 1\,. \tag{3.17b}$$

We remark that the limiting expression (3.17a) is not uniformly valid as $s \to 1^+$.

We now illustrate our result for the GM exponent set $(p,q,m,s) = (3,2,3,0)$. We obtain from (3.14) and (3.16) that

$$\tau = \frac{1}{3\omega_0}\left(\frac{81}{(1+\omega_0^2)^2} - 1\right)^{1/2}, \qquad \lambda_{IH} = \omega_0/3\,, \qquad \text{for} \quad \sqrt{3\sqrt{17}-11}/\sqrt{2} \leq \omega_0 \leq 2\sqrt{2}\,, \tag{3.18a}$$

$$T = \frac{1}{3\omega_0}\tan^{-1}\left(\frac{\omega_0 B_+/B_- - 1}{B_+/B_- + \omega_0}\right), \qquad \frac{B_+}{B_-} = \sqrt{\frac{10+\omega_0^2}{8-\omega_0^2}}\,. \tag{3.18b}$$

In this way, in the left panel of Fig. 3.1 we plot the Hopf bifurcation boundary in the τ versus T plane. Alternatively, for the exponent set $(p, q, m, s) = (3, 2, 3, 1)$, for which $s = 1$, there is no longer any Hopf bifurcation value of $T > 0$ when $\tau = 0$. For this case, a plot of the stability boundary in the τ versus T plane, as computed from (3.14) and (3.16) is shown in the right panel of Fig. 3.1, together with the limiting approximation given in (3.17b), which is valid for $\tau \to 0^+$.

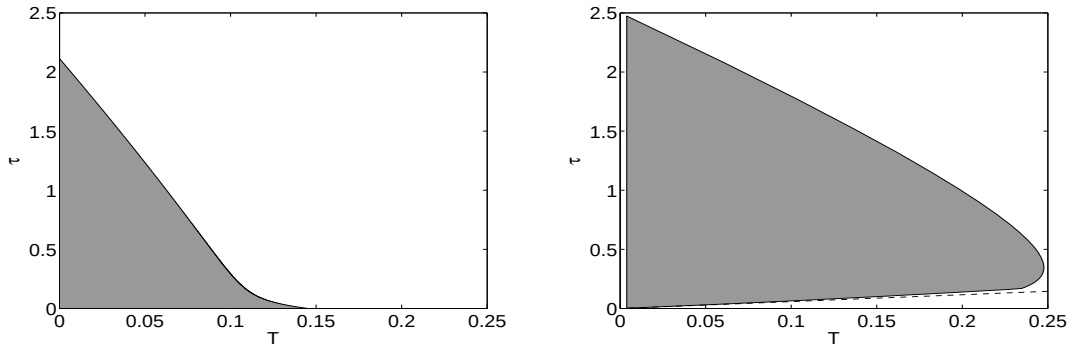

Fig. 3.1: The stable shaded region in the τ versus T plane for a one-spike solution to the infinite-line problem (3.1), with delay only in the inhibitor, as governed by the NLEP (3.9). Left: the exponent set $(p, q, m, s) = (3, 2, 3, 0)$. The boundary of the shaded region is given in (3.18). Right: $(p, q, m, s) = (3, 2, 3, 1)$. The boundary of the shaded region is given by (3.14) and (3.16). The dashed line is the limiting approximation (3.17b) valid for $\tau \to 0$.

For the exponent set $(p, q, m, s) = (3, 2, 3, 0)$ in the left panel of Fig. 3.2 we plot the other Hopf bifurcations that occur for the larger values of T given by $T_n = T + 2\pi n/(3\omega_0)$ for $n \geq 1$, with n an integer, where T is given in (3.18), together with the curve where real roots of (3.10) first occur. Additionally, we can fix a value of τ and calculate the path of the eigenvalues as T ranges from its first Hopf bifurcation point T_0 to some large value of T. Setting $\tau = 1$ in (3.10), and by computing the roots of (3.10) numerically, in the right panel of Fig. 3.2 we plot the path of some of the eigenvalues in the unstable half-plane $\mathrm{Re}(\lambda) > 0$ as T increases. The eigenvalue path for the primary Hopf bifurcation hits the real axis at $T \approx 0.8239$, with one eigenvalue tending to the origin while the other tending to $\lambda = \beta = 3$ as T increases. In the right panel of Fig. 3.2 other eigenvalue branches are shown, and these branches tend to the origin as T increases.

To characterize this behavior observed in Fig. 3.2, we first analyze the roots of (3.10) on the positive real axis. For simplicity we will consider only the case $s = 0$. We write (3.10) as

$$\sqrt{1 + \tau\lambda} = \mathcal{K}(\lambda) \equiv \frac{m^2 q}{2(\beta - \lambda)} e^{-\lambda T}\,, \qquad \beta = m^2 - 2m\,. \tag{3.19}$$

We first observe that $\sqrt{1 + \tau\lambda}$ is a monotone increasing concave function of λ. For the right-hand side of (3.19) we calculate that $\mathcal{K}(0) = 1 + \xi > 1$ and $\mathcal{K}(\lambda) \to +\infty$ as $\lambda \beta^-$. Moreover, after a little algebra, we calculate that

$$\mathcal{K}'(\lambda) = \frac{m^2 q}{2(\beta - \lambda)^2} e^{-\lambda T} \left[1 - (\beta - \lambda)T\right]\,, \qquad \mathcal{K}''(\lambda) = \frac{\beta(\xi + 1)}{(\beta - \lambda)^3} e^{-\lambda T} \left[(T(\beta - 1) - 1)^2 + 1\right] > 0\,. \tag{3.20}$$

Therefore, $\mathcal{K}''(\lambda) > 0$ on $0 < \lambda < \beta$ and $\mathcal{K}'(\lambda) = 0$ at $\lambda_{\min} = \beta\,(1 - 1/T) < \beta$. As such, we conclude that (3.19) has exactly two real roots on $0 < \lambda < \beta$ whenever T is large enough so that $\mathcal{K}_{\min} = \mathcal{K}(\lambda_{\min}) < 1$. To determine the precise value of T for which a double real root of (3.19) occurs we simply require that (3.19) holds together with the tangency condition $\tau(1 + \tau\lambda)^{-1/2}/2 = \mathcal{K}'(\lambda)$. As τ is varied for the exponent set $(p, q, m, s) = (3, 2, 3, 0)$ the double root value for T is shown by the heavy solid curve in the left panel of Fig. 3.2.

Next, we follow the procedure in §2.1 to determine the spectrum near the origin for the NLEP (3.9) in the limit of large delay T. The determination of the limiting asymptotics follows precisely that given in (2.7)–(2.12) except that we

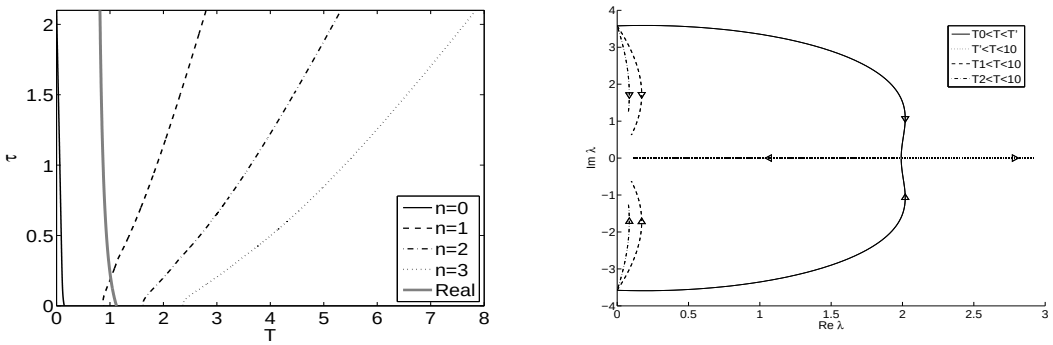

Fig. 3.2: The infinite-line problem (3.1) for the exponent set $(p,q,m,s)=(3,2,3,0)$, with delay only in the inhibitor, characterized by the NLEP (3.9). Left: Hopf bifurcation curves (dashed curves) are shown corresponding to where additional complex conjugate pairs, indexed by n, enter the region $\mathrm{Re}(\lambda)>0$. The thick line corresponds to when eigenvalues for (3.1) first appear as a double root on the positive real axis. Right: Eigenvalue paths for $\tau=1$. The description of this plot is identical to that in the caption of Fig. 2.2. The heavy solid curve is the eigenvalue path associated with the primary Hopf bifurcation on the interval $T\in[T_0,T']$, where $T_0\approx 0.0626$ is the primary Hopf bifurcation point and $T'\approx 0.8239$ is where the first real eigenvalue appears. For $T>T'$ one eigenvalue tends to the origin, whereas the other eigenvalue tends to $\lambda=\beta=3$ as T increases. In addition, $T_1\approx 1.8186$ and $T_2\approx 3.5746$ are where additional Hopf bifurcations occur.

must replace τ by $\tau/2$ since $\sqrt{1+\tau\lambda}\approx 1+\tau\lambda/2+\cdots$ for $\lambda\ll 1$. In this way, in place of (2.12) we obtain that

$$\lambda\sim\frac{c_0}{T}\left(1+\frac{f}{T}+\cdots\right),\qquad f=-\frac{\tau}{2}+\frac{mq}{(p-1)^2(1+\xi)}\left(1-\frac{(p-1)}{2m}\right), \tag{3.21}$$

where $c_0\equiv\ln(1+\xi)+2n\pi i$ with $n=0,1,2,\ldots$. For the exponent set $(p,q,m,s)=(3,2,3,0)$ of Fig. 3.2, (3.21) reduces to

$$\lambda\sim\frac{[\ln 3+2n\pi i]}{T}\left(1+\frac{1}{T}\left[\frac{1}{3}-\frac{\tau}{2}\right]++\cdots\right). \tag{3.22}$$

Therefore, branches of eigenvalues tend to the origin as T increases, as seen in the right panel of Fig. 3.2.

3.2. Inhibitor Delay: The Infinite-Line Problem for Arbitrary GM Exponent Sets. In this subsection we use the NLEP (3.9) to compute the Hopf bifurcation boundary in the τ versus T plane for a one-spike solution to the 1-D infinite-line problem (3.1) for an arbitrary exponent set (p,q,m,s) satisfying (1.1b). In analogy with (2.34), and with $w(y)$ defined by (2.3) and $L_0\Phi\equiv\Phi''-\Phi+pw^{p-1}\Phi$, the discrete eigenvalues of the NLEP (3.9) must be the roots of

$$\frac{1}{mq}\left[e^{\lambda T}\sqrt{1+\tau\lambda}+s\right]=\mathcal{F}(\lambda),\qquad\text{where}\qquad\mathcal{F}(\lambda)\equiv\frac{\int_{-\infty}^{\infty}w^{m-1}\left[(L_0-\lambda)^{-1}w^p\right]\,dy}{\int_{-\infty}^{\infty}w^m\,d\rho}. \tag{3.23}$$

To determine the Hopf bifurcation boundaries we set $\lambda=i\lambda_{IH}$ in (3.23) and separate real and imaginary parts to get

$$e^{i\lambda_{IH}T}=\frac{(B_+-iB_-)}{B_+^2+B_-^2}\left(-s+mq\mathcal{F}_R+imq\mathcal{F}_I\right), \tag{3.24}$$

where $\mathcal{F}(i\lambda_{IH})=\mathcal{F}_R(\lambda_{IH})+i\mathcal{F}_I(\lambda_{IH})$, and $\sqrt{1+i\tau\lambda_{IH}}=B_++iB_-$, where $B_\pm$ are defined in (3.12). We have

$$\mathcal{F}_R(\lambda_{IH})\equiv\frac{\int_{-\infty}^{\infty}w^{m-1}L_0\left[L_0^2+\lambda_{IH}^2\right]^{-1}w^p\,dy}{\int_{-\infty}^{\infty}w^m\,dy},\qquad\mathcal{F}_I(\lambda_{IH})\equiv\frac{\lambda_{IH}\int_{-\infty}^{\infty}w^{m-1}\left[L_0^2+\lambda_{IH}^2\right]^{-1}w^p\,dy}{\int_{-\infty}^{\infty}w^m\,dy}. \tag{3.25}$$

By taking the modulus of both sides of (3.24) we obtain that

$$\tau^2\lambda_{IH}^2=\mathcal{N}_i(\lambda_{IH})\equiv\left[(mq\mathcal{F}_R-s)^2+(mq\mathcal{F}_I)^2\right]^2-1,$$

provided that $\mathcal{N}_i(\lambda_{IH}) > 0$. Then, by taking the imaginary part of (3.24), restricted to the range of λ_{IH} for which $\mathcal{N}_i(\lambda_{IH}) > 0$, we obtain the following parametric representation of the Hopf bifurcation boundary in the τ versus T plane:

$$\tau \equiv \frac{1}{\lambda_{IH}}\sqrt{\mathcal{N}_i(\lambda_{IH})}\,, \qquad T \equiv \frac{1}{\lambda_{IH}}\sin^{-1}\left(\frac{mqB_+\mathcal{F}_I + B_-(s-mq\mathcal{F}_R)}{\sqrt{1+\mathcal{N}_i(\lambda_{IH})}}\right). \tag{3.26}$$

When $s < 1$, we can readily prove, as was done for the shadow problem studied in §2.3, that there is a Hopf bifurcation value of T when $\tau = 0$. To prove this we use $\mathcal{F}_R(0) = 1/(p-1)$ and $\mathcal{F}_I(0) = 0$, together with $\mathcal{F}_R(\lambda_I) = \mathcal{O}(\lambda_{IH}^{-2})$ and $\mathcal{F}_I(\lambda_I) = \mathcal{O}(\lambda_{IH}^{-1})$ as $\lambda_{IH} \to \infty$ (cf. [22]). This yields that $\mathcal{N}_i(0) = (\xi+1)^4 - 1 > 0$ and $\mathcal{N}_i \to s^4 - 1 < 0$ as $\lambda_{IH} \to \infty$. Therefore, there is a root $\lambda_{IH} = \lambda_{IH}^f$ to $\mathcal{N}_i(\lambda_{IH}) = 0$. Then, by using (3.26) for T, the Hopf bifurcation value of the delay is the same as given in (2.37b). Therefore, we conclude for the 1-D infinite-line problem that whenever $s < 1$ there must be a Hopf bifurcation value of the delay when $\tau = 0$ for any GM exponent set satisfying (1.1b).

In the right panel of Fig. 1.1 we use the parametrization (3.26) to calculate the Hopf bifurcation curve in the τ versus T plane for the infinite-line problem for the prototypical GM exponent set $(p,q,m,s) = (2,1,2,0)$. The numerical procedure to compute $\mathcal{F}_R(\lambda_{IH})$ and $\mathcal{F}_I(\lambda_{IH})$ are as described in §2.3.

Finally, we remark that we can determine the spectrum of the NLEP (2.32) near the origin for large delay T. We readily derive, in analogy with (2.12) for the 1-D shadow problem, that

$$\lambda \sim \frac{c_0}{T}\left(1 + \frac{f}{T} + \cdots\right), \qquad f = -\frac{\tau}{2} + \frac{mq}{(p-1)^2(\xi+1)}\left(1 - \frac{(p-1)}{2m}\right). \tag{3.27}$$

Here $c_0 = \ln(1+\xi) + 2n\pi i$, with $n = 0, \pm 1, \pm 2, \ldots$. This expression is identical to that derived in (2.12) for the 1-D shadow problem apart from the factor of $1/2$ in τ.

3.3. Comparison with Full Numerics. In order to compare our stability theory with results from full-scale numerical computations, we consider the GM model for the exponent set $(p,q,m,s) = (3,2,3,0)$ with delayed inhibitor kinetics on the finite domain $|x| \le L$, formulated as

$$v_t = \varepsilon^2 v_{xx} - v + v^3/u_T^2\,, \qquad \tau u_t = u_{xx} - u + \varepsilon^{-1}v^3\,; \qquad u_x(\pm L,t) = v_x(\pm L,t) = 0\,, \tag{3.28}$$

where $u_T \equiv u(x,t-T)$. The steady-state one-spike solution for (3.28) is given in Principal Result 3.1 with $m = 3$, $\gamma = 1$, and where the Green's function $G_0(x)$ satisfies $G_{0xx} - G_0 = -\delta(x)$ in $|x| \le L$ with $G_{0x}(\pm L) = 0$.

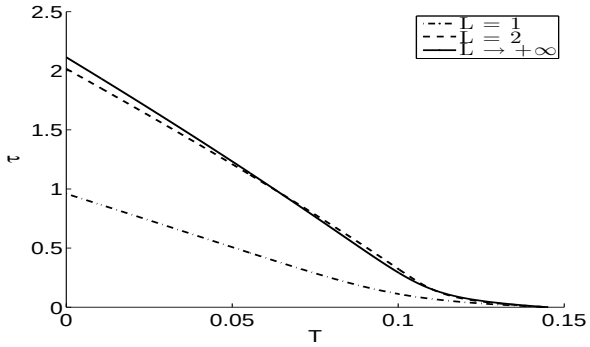

Fig. 3.3: The stability regions in the τ versus T plane for a one-spike solution to the finite-line problem (3.28) with GM exponent set $(3,2,3,0)$, with delay only in the inhibitor, on a domain of length $2L$ with $L = 1, 2$. The result for the infinite line problem is also shown. The boundary of the shaded regions are computed using (3.29).

To analyze the linear stability of the one-spike steady-state on an $\mathcal{O}(1)$ time-scale we proceed as for the infinite-line problem, noting that the NLEP with this exponent set is explicitly solvable. We readily derive that the eigenvalues of the NLEP satisfy the transcendental equation

$$\lambda = 3 - 9\frac{e^{-\lambda T}}{\sqrt{1+\tau\lambda}}\left(\frac{\tanh\theta(0)}{\tanh\theta(\lambda)}\right), \qquad \theta(\lambda) \equiv \frac{L\sqrt{1+\tau\lambda}}{\sqrt{D}}. \tag{3.29}$$

If we let $L \to \infty$ in (3.29) we recover (3.19) with $m = 3$ and $q = 2$. By setting $\lambda = i\omega_0$ in (3.29), and equating the real and imaginary parts of (3.29) to zero, we obtain a parameterization of the stability boundary in the τ versus T plane where a Hopf bifurcation occurs. This numerically computed boundary is shown in Fig. 3.3 for $L = 1$, $L = 2$, and $L = \infty$.

Next, we compare results from the stability diagram Fig. 3.3 with full numerical results computed from (3.28). To numerically solve (3.28), we used a method of lines approach that approximated the spatial derivatives in (3.28) with centered differences and used the dde23 solver of Matlab to solve the system of delay (ordinary) differential equations (DDEs). To generate a more precise initial condition than the asymptotic one-spike steady-state solution of Principal Result 3.1 we used this asymptotic spike profile as an initial guess for the Matlab bvp4c solver. This numerically computed steady-state was used as the initial functions on the interval $t \in [-T, 0)$. The computations shown in Fig. 3.4 for the spike amplitude $v(0,t)$ versus t used 151 spatial meshpoints for both u and v, and the parameter set $\epsilon = 0.05$, $L = 2$, time delay $T = 0.05$, and the GM exponent set $(p, q, m, s) = (3, 2, 3, 0)$. With this parameter set, the phase diagram Fig. 3.3 predicts a Hopf bifurcation when $\tau = \tau_H \approx 1.23$, and that the spike is linearly stable only when $\tau < \tau_H$. In the left panel of Fig. 3.4 where $\tau = 1.0$, we observe that the oscillation amplitude slowly decreases in time, whereas from the right panel of Fig. 3.4, where $\tau = 1.3$, we observe uncontrolled temporal oscillations of the spike amplitude, suggesting that the Hopf bifurcation is in fact subcritical. Although, as a result of of prohibitive computational expense of solving large systems of delay differential equations, we were unable to resolve the Hopf bifurcation threshold more precisely by increasing the number of spatial meshpoints, the results in Fig. 3.4 are entirely consistent with our linear stability predictions.

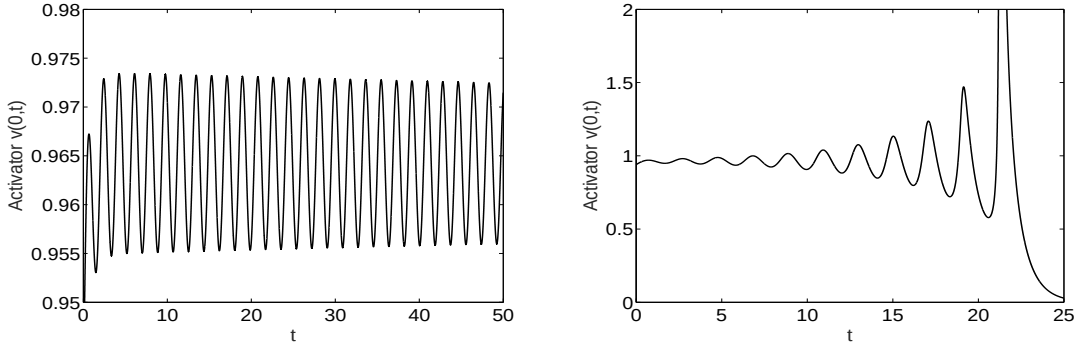

Fig. 3.4: Full numerical results for the spike amplitude $v(0,t)$ versus t for (3.28) with $\epsilon = 0.05$, $L = 2$, $T = 0.05$, and $(p, q, m, s) = (3, 2, 3, 0)$. Left panel: $\tau = 1.0$, showing slowly decaying oscillations. Right panel: $\tau = 1.3$ showing large-scale uncontrolled oscillations beyond the Hopf bifurcation value $\tau_H \approx 1.23$.

4. Delay Effects for an N-Spot Pattern in a Finite 2-D Domain. In this section, we determine stability thresholds for an M-spot pattern for the GM model, with $M > 1$, for the prototypical exponent set $(p, q, m, s) = (2, 1, 2, 0)$ with delayed inhibitor kinetics in a bounded 2-D domain Ω. This problem is formulated as

$$v_t = \varepsilon^2\Delta v - v + \frac{v^2}{u_T}, \quad \mathbf{x} \in \Omega; \qquad \tau u_t = D\Delta u - u + \frac{1}{\varepsilon^2}v^2, \quad \mathbf{x} \in \Omega; \qquad \partial_n u = \partial_n v = 0, \quad \mathbf{x} \in \partial\Omega. \tag{4.1}$$

A localized spot pattern is one for which the steady-state solution for v concentrates at a discrete set of points $\mathbf{x}_j \in \Omega$, for $j = 1, \dots, M$, as $\epsilon \to 0$. In [26], the linear stability properties of such patterns were analyzed in the weak coupling regime where $D = \mathcal{O}(\nu^{-1})$ where $\nu = -1/\ln\epsilon$. Here we extend this analysis to allow for the effect of delayed inhibitor kinetics. By setting $D = D_0/\nu$ in (4.1), we can readily extend the analysis of [26] to show that, with a delayed inhibitor kinetics, the linear stability of an N-spot solution is determined by the spectrum of the following NLEP:

$$L_0\Phi - \chi w^2 \frac{\int_0^\infty \rho w \Phi \, d\rho}{\int_0^\infty \rho w^2 \, d\rho} = \lambda \Phi \,, \qquad \Phi \to 0 \quad \text{as} \quad \rho \to \infty \,; \qquad L_0\Phi \equiv \Delta_\rho \Phi - \Phi + 2w\Phi \,, \tag{4.2a}$$

where $\Delta_\rho \equiv \partial_{\rho\rho}\Phi + \rho^{-1}\partial_\rho \Phi$ is the radially symmetric part of the Laplacian, and $w(\rho) > 0$ is the ground-state solution obtained by setting $p = 2$ in (2.31). In (4.2a), there are two possible choices for the multiplier χ, corresponding to either synchronous or asynchronous perturbations near each localized spot, denoted by χ_s and χ_a, respectively (cf. [26]):

$$\chi_a \equiv \frac{2e^{-\lambda T}}{1+\mu} \,, \qquad \chi_s \equiv \chi_a \left(1 + \frac{\mu}{1+\tau\lambda}\right) \,, \qquad \mu \equiv \frac{2\pi M D_0}{|\Omega|} \,, \qquad D = \frac{D_0}{\nu} \,, \qquad \nu = -\frac{1}{\ln\varepsilon} \,, \tag{4.2b}$$

where $|\Omega|$ is the area of Ω. With either choice of the multiplier, the discrete eigenvalues of the NLEP are roots of

$$\frac{1}{\chi(\lambda)} = \mathcal{F}(\lambda) \,; \qquad \mathcal{F}(\lambda) \equiv \frac{\int_0^\infty \rho w \left[(L_0 - \lambda)^{-1} w^2\right] \, d\rho}{\int_0^\infty \rho^{N-1} w^2 \, d\rho} \,. \tag{4.3}$$

The following lemma will be used to determine the behavior of the eigenvalues of (4.2) in the large delay limit $T \gg 1$:

Lemma 4.1. *Consider the NLEP*

$$L_0\Phi - \tilde{\chi}(\lambda) e^{-\lambda T} w^2 \frac{\int_0^\infty \rho w \Phi \, d\rho}{\int_0^\infty \rho w^2 \, d\rho} = \lambda \Phi \,, \tag{4.4}$$

with $\Phi \to 0$ as $\rho \to \infty$, where $\tilde{\chi}(\lambda)$ has asymptotics $\tilde{\chi}(\lambda) \sim \tilde{\chi}_0 + \lambda\tilde{\chi}_1 + \cdots$ as $\lambda \to 0$. Then, for $T \gg 1$, the eigenvalues of (4.4) near the origin have the limiting asymptotics

$$\lambda \sim \frac{c_0}{T} + \frac{c_0}{T^2}\left[\frac{\tilde{\chi}_1}{\tilde{\chi}_0} + \frac{1}{2}\right] + \cdots \,; \qquad c_0 = \ln(\chi_0) + 2n\pi i \,, \quad n = 0, \pm 1, \pm 2, \dots \,. \tag{4.5}$$

Proof. To establish this result, we proceed in a similar way as done in (2.8)–(2.12). We set $\lambda T = c$ with $T \gg 1$, and use $\tilde{\chi} \sim \tilde{\chi}_0 + (c/T)\,\tilde{\chi}_1 + \cdots$, and expand $c = c_0 + c_1/T + \cdots$. From (4.4) we derive that

$$L_0\Phi - e^{-c_0}\left(\tilde{\chi}_0 + \frac{1}{T}\left(c_0\tilde{\chi}_1 - c_1\tilde{\chi}_0\right) + \cdots\right) w^2 \frac{\int_0^\infty \rho w \Phi \, d\rho}{\int_0^\infty \rho w^2 \, d\rho} = \frac{c_0}{T}\Phi + \cdots \,. \tag{4.6}$$

Then, we use the identity $L_0 w = w^2$ and expand $\Phi = w + (1/T)\,\Phi_1 + \cdots$. This yields that $e^{-c_0}\tilde{\chi}_0 = 1$, and that

$$L_0\Phi_1 - w^2 \frac{\int_0^\infty \rho w \Phi_1 \, d\rho}{\int_0^\infty \rho w^2 \, d\rho} = w^2\left(\frac{c_0\tilde{\chi}_1}{\tilde{\chi}_0} - c_1\right) + c_0 w \,. \tag{4.7}$$

By imposing the solvability condition for (4.7), as done in (2.39), we calculate $c_1 = c_0\,(\tilde{\chi}_1/\tilde{\chi}_0 + 1/2)$. This yields (4.5). □

4.1. The Competition or Asynchronous Modes. We first examine (4.2) with $\chi = \chi_a$. With no delay, i.e. $T = 0$, the rigorous results of [26] prove that $\mathrm{Re}(\lambda) < 0$ if and only if $\mu < 1$, i.e. if and only if the number of spots satisfies $M < |\Omega|/(2\pi D_0)$. Moreover, there is a unique unstable real positive eigenvalue for any $\mu > 1$.

To consider the effect of delay, we set $\chi = \chi_a$ in (4.3), and let $\lambda = i\lambda_{IH}$ with $\lambda_{IH} > 0$. Upon separating (4.3) into real and imaginary parts, we readily derive that at a Hopf bifurcation λ_{IH} must be a root of

$$\frac{(\mu+1)^2}{4} = \mathcal{M}(\lambda_{IH}) \equiv \left[\mathcal{F}_R(\lambda_{IH})\right]^2 + \left[\mathcal{F}_I(\lambda_{IH})\right]^2 \,, \tag{4.8a}$$

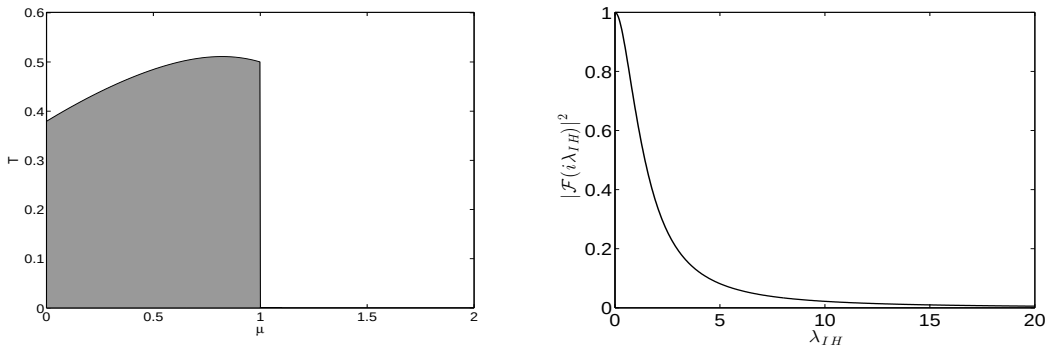

Fig. 4.1: Left panel: the Hopf bifurcation boundary and the region of linear stability in the T versus μ plane for the asynchronous mode for an M-spot pattern of (4.1) in the regime $D = \mathcal{O}(\nu^{-1})$. Right panel: plot of $\mathcal{M}(\lambda_{IH}) = |\mathcal{F}(i\lambda_{IH})|^2$ versus λ_{IH}, which establishes that there is a Hopf bifurcation value of the delay whenever $0 < \mu < 1$, where $\mu = 2\pi M D_0/|\Omega|$.

where $\mathcal{F}_R(\lambda_{IH})$ and $\mathcal{F}_I(\lambda_{IH})$ are obtained by setting $N = 2$ and $p = m = 2$ in (2.34b). Since $\mathcal{F}_R(0) = 1$, $\mathcal{F}_I(0) = 0$, while $\mathcal{F}_R \to 0$ and $\mathcal{F}_I \to 0$ as $\lambda_{IH} \to \infty$, the intermediate value theorem yields that there is a root to (4.8a) whenever $0 < \mu < 1$. As proved in §2 of [22] we have $\mathcal{F}_R(\lambda_{IH}) > 0$ and $\mathcal{F}_R(\lambda_{IH}) > 0$ for all $\lambda_{IH} > 0$. Moreover, from the right panel of Fig. 4.1, where we plot the numerically computed $\mathcal{M}(\lambda_{IH})$ versus λ_{IH}, we observe that $\mathcal{M}(\lambda_{IH})$ is monotone decreasing and satisfies $0 < \mathcal{M}(\lambda_{IH}) < 1$. Thus, there is no root to (4.8a), and hence no Hopf bifurcation, when $\mu > 1$. In contrast, for any μ in $0 < \mu < 1$, there is a unique root to (4.8a), and the corresponding minimum value of the delay is

$$T = \frac{1}{\lambda_{IH}} \tan^{-1}\left(\frac{\mathcal{F}_I(\lambda_{IH})}{\mathcal{F}_R(\lambda_{IH})}\right). \tag{4.8b}$$

A plot of (4.8b) versus μ on $0 < \mu < 1$, together with the shaded region where the spot pattern is linearly stable, is shown in the left panel of Fig. 4.1. As a remark, since $\mathcal{F}_I(\lambda_{IH}) \sim \lambda_{IH}/2$ as $\lambda_{IH} \to 0$ and $\mathcal{F}_R(0) = 1$ (cf. [22]), we predict from (4.8b) that $T \sim 1/2$ as $\mu \to 1^-$. This limiting value is indeed confirmed from the left panel of Fig. 4.1.

Next, we use (4.5) of Lemma 4.1 with $\tilde{\chi}_0 = 2/(1+\mu)$ and $\tilde{\chi}_1 = 0$ to establish, for large delay T, that the eigenvalues near the origin have the limiting asymptotics

$$\lambda \sim \frac{c_0}{T}\left[1 + \frac{1}{2T}\right], \quad \text{as} \quad T \to +\infty\,; \qquad c_0 = -\ln\left(\frac{1+\mu}{2}\right) + 2n\pi i\,. \tag{4.9}$$

We conclude that when $\mu > 1$, where no Hopf bifurcation value of T occurs, we have $\mathrm{Re}(c_0) < 0$ and so as $T \to \infty$ the eigenvalues approach the origin from the stable left-half plane $\mathrm{Re}(\lambda) < 0$. In contrast, when $0 < \mu < 1$, we have $\mathrm{Re}(c_0) > 0$, and so as $T \to \infty$ the eigenvalues approach the origin from the unstable half-plane $\mathrm{Re}(\lambda) > 0$. We note that the eigenvalue with $n = 0$ is real and tends to the origin as $T \to +\infty$.

Finally, we determine the behavior of the eigenvalues on the positive real axis. For $\lambda > 0$ real, we write (4.3) as

$$\frac{(1+\mu)}{2} e^{\lambda T} = \mathcal{F}(\lambda)\,, \tag{4.10}$$

where $\mathcal{F}(\lambda)$ is defined in (4.3). As proved in [22] we have that $\mathcal{F}(0) = 1$, $\mathcal{F}'(\lambda) > 0$ on $0 < \lambda < \sigma_0$, where $\sigma_0 \approx 1.648$ is the principal eigenvalue of L_0. Moreover, it was shown in [22] that $\mathcal{F}'(\lambda) > 0$ on $0 < \lambda < \sigma_0$. We further note that the left-hand side of (4.10) begins at $(1+\mu)/2$, and is monotone increasing convex function in λ for $T > 0$. As such, when $0 < \mu < 1$, there are two real roots to (4.10) on the interval $0 < \lambda < \sigma_0$ when T is large enough. As $T \to \infty$, one of these roots tends to the origin $\lambda = 0$. This root corresponds to the limiting asymptotics result (4.9) with $n = 0$ and $T \gg 1$. In contrast, when $\mu > 1$, there is a unique root to (4.10) on $0 < \lambda < \sigma_0$ for any $T > 0$. This root tends to σ_0 as $T \to +\infty$.

4.2. The Synchronous Mode. Next, we study (4.2) with $\chi = \chi_s$. From (4.3), the eigenvalues of the NLEP satisfy

$$\frac{e^{\lambda T}}{2}(1+\mu)\left(\frac{1+\tau\lambda}{\mu+1+\tau\lambda}\right) = \mathcal{F}(\lambda)\,, \tag{4.11}$$

where $\mathcal{F}(\lambda)$ is defined in (4.3). To determine the Hopf bifurcation boundary we set $\lambda = i\lambda_{IH}$ with $\lambda_{IH} > 0$, to obtain

$$e^{i\lambda_{IH}T} = \frac{2}{\mu+1}\left(\frac{\mu+1+i\tau\lambda_{IH}}{1+i\tau\lambda_{IH}}\right)\mathcal{F}(i\lambda_{IH})\,. \tag{4.12}$$

By setting the modulus of the right hand side to unity, and then solving for τ, we conclude that

$$\tau = \frac{(\mu+1)}{\lambda_{IH}}\left(\frac{4|\mathcal{F}|^2-1}{(\mu+1)^2-4|\mathcal{F}|^2}\right)^{1/2}, \qquad \text{for} \quad \frac{1}{4} \le |\mathcal{F}|^2 < \frac{(\mu+1)^2}{4}\,, \tag{4.13}$$

where $|\mathcal{F}|^2 \equiv (\mathcal{F}_R(\lambda_{IH}))^2 + (\mathcal{F}_I(\lambda_{IH}))^2$. From the plot of $|\mathcal{F}|^2$ versus λ_{IH} shown in the right panel of Fig. 4.1, the range of $|\mathcal{F}|^2$ required in (4.13) implicitly specifies a range of λ_{IH}. To determine the minimum value of the delay T for a Hopf bifurcation, we then separate (4.12) into real and imaginary parts. After a short calculation we obtain that

$$T = \frac{1}{\lambda_{IH}}\sin^{-1}\left(\frac{2}{(\mu+1)(1+\tau^2\lambda_{IH}^2)}\left((\mu+1+\tau^2\lambda_{IH}^2)\mathcal{F}_I - \tau\lambda_{IH}\mu\mathcal{F}_R\right)\right)\,. \tag{4.14}$$

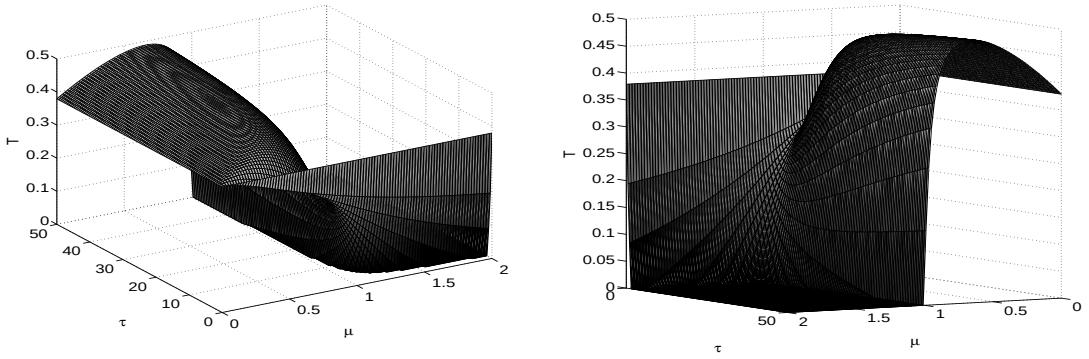

Fig. 4.2: Two views of the Hopf bifurcation surface in the (τ, T, μ) space for the synchronous mode for an M-spot pattern of (4.1) in the regime $D = \mathcal{O}(\nu^{-1})$. Any triple (τ, T, μ) that lies below this surface is linearly stable.

For a fixed value of μ, the coupled system (4.13) and (4.14) specifies a curve in the τ versus T plane parametrized by λ_{IH}. By varying μ, we then obtain a surface in the (τ, T, μ) space at which a Hopf bifurcation occurs. By using (2.34b) with $N = 2$ and $p = m = 2$ to compute $\mathcal{F}_R$ and $\mathcal{F}_I$ numerically, in Fig. 4.2 we give two different views of the Hopf bifurcation surface in the (τ, T, μ) plane. We now explain some of the qualitative features of this surface.

We first characterize the Hopf bifurcation boundary when $T = 0$. The left panel of Fig. 4.2 suggests that $\mu = 1$ is a critical threshold. With no delay, we obtain from the real and imaginary parts of (4.12) that

$$(\mu+1+\tau^2\lambda_{IH}^2)\mathcal{F}_I = \tau\lambda_{IH}\mu\mathcal{F}_R\,, \qquad \frac{2}{(\mu+1)(1+\tau^2\lambda_{IH}^2)}\left[(\mu+1+\tau^2\lambda_{IH}^2)\mathcal{F}_R + (\mu+1)\tau\lambda_{IH}\mathcal{F}_I - \tau\lambda_{IH}\mathcal{F}_I\right] = 1\,. \tag{4.15}$$

To decouple (4.15), we solve the second equation for $(\mu+1)$, and then eliminate this quantity by using the first equation. This yields a cubic equation for τ, which can be factored as $(1+\tau^2\lambda_{IH}^2)\left(\tau\lambda_{IH}\mathcal{F}_I - 2|\mathcal{F}|^2 + \mathcal{F}_R\right) = 0$. This determines τ. We then determine μ from the first equation of (4.15) by eliminating τ. In this way, we obtain for the case of no delay that the Hopf bifurcation boundary in the τ versus μ plane, as parameterized by $\lambda_{IH} > 0$, is

$$\tau = \frac{1}{\lambda_{IH}\mathcal{F}_I}\left(2|\mathcal{F}|^2 - \mathcal{F}_R\right)\,, \qquad \mu = \frac{(2\mathcal{F}_R-1)^2 + 4\mathcal{F}_I^2}{2\mathcal{F}_R - 1}\,, \tag{4.16}$$

on the range of $\lambda_{IH} > 0$ for which $\tau > 0$ and $\mu > 0$.

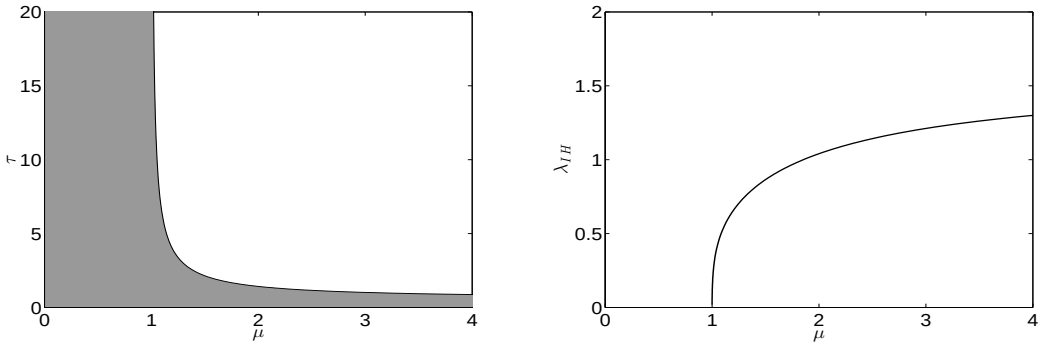

Fig. 4.3: Left panel: the Hopf bifurcation boundary and the region of linear stability in the τ versus μ plane for the synchronous mode for an M-spot pattern of (4.1) in the regime $D = \mathcal{O}(\nu^{-1})$ assuming no delay in the inhibitor kinetics, i.e. $T = 0$. Right panel: the corresponding Hopf bifurcation frequency λ_{IH} versus μ with no delay.

By computing $\mathcal{F}_R$ and $\mathcal{F}_I$ numerically, in Fig. 4.3 we use (4.16) to plot the Hopf bifurcation threshold τ and the corresponding frequency λ_{IH} versus μ. We observe that a Hopf bifurcation occurs only when $\mu > 1$, and that $\tau \to +\infty$ and $\lambda_{IH} \to 0^+$ as $\mu \to 1^+$. Since $\mathcal{F}_I \sim \lambda_{IH}/2$ and $\mathcal{F}_R \sim 1 + \mathcal{O}(\lambda_{IH}^2)$ as $\lambda_{IH} \to 0^+$ from [22], we conclude from (4.16) that $\tau \sim 2/\lambda_{IH}^2$ as $\lambda_{IH} \to 0$, or equivalently $\tau = \mathcal{O}\left(1/(\mu - 1)\right)$ as $\mu \to 1^+$. Alternatively, as $\lambda_{IH} \to \lambda_{IH}^0$ from below, where $\lambda_{IH}^0 \approx 1.59$ is the unique root of $\mathcal{F}_R(\lambda_{IH}) = 1/2$, we conclude from (4.16) that $\tau \to \tau_\infty \equiv \frac{2}{\lambda_{IH}^0} 2\mathcal{F}_I(\lambda_{IH}^0)/\lambda_{IH}^0 \approx 0.563$ as $\mu \to +\infty$. These results explain the behavior of the Hopf bifurcation surface $T = 0$ shown in the left panel of Fig. 4.2.

A second qualitative feature that is evident from Fig. 4.2 is that there is a Hopf bifurcation value of T when $\tau = 0$ that is independent of μ. To show this analytically, we set $\tau = 0$ in (4.12) to obtain that this threshold, denoted by T^f, and the corresponding frequency λ_{IH}^f satisfy $e^{i\lambda_{IH}T} = 2\mathcal{F}_R(\lambda_{IH}) + 2i\mathcal{F}_I(\lambda_{IH})$, which is independent of μ. Therefore, λ_{IH} satisfies $\mathcal{F}_R^2 + \mathcal{F}_I^2 = 1/4$, which yields $\lambda_{IH}^f \approx 2.55$. The corresponding value of the delay $T^f = (\lambda_{IH}^f)^{-1} \tan^{-1}\left(\mathcal{F}_I/\mathcal{F}_R\right) \approx 0.379$, confirms the horizontal line in the right panel of Fig. 4.2 in the $\tau = 0$ plane. This critical value T^f separates the stability boundary surface into two sections. For $0 < T < T^f$, the Hopf bifurcation boundary in the τ versus μ plane has $\tau \to \tau_\infty \approx 0.563$ as $\mu \to \infty$, while $\tau \to \infty$ as $\mu \to 1$, and the region of stability is to the left of the curve. For $T^f < T < T_{\max}$, the contour created is parabolically shaped, with $\tau \to \infty$ as $\mu \to 0$ or $\mu \to 1$, and the region of linear stability lies above the curve. In Fig. 4.4 these differences are shown in the plots of τ versus μ for four separate values of the delay T. These plots are obtained numerically by using Newton's method on (4.13) and (4.14).

Next, we calculate the large delay behavior of the roots to the NLEP (4.2) for the synchronous mode. Since $\tilde{\chi}_0 = 2$ and $\tilde{\chi}_1 = -2\mu\tau/(\mu + 1)$, we obtain from (4.5) of Lemma 4.1 that the eigenvalues near the origin have the limiting asymptotics

$$\lambda \sim \frac{c_0}{T}\left[1 + \frac{1}{T}\left(\frac{1}{2} - \frac{\mu\tau}{1+\mu}\right)\right], \quad \text{as} \quad T \to +\infty\,; \qquad c_0 = \ln 2 + 2n\pi i\,. \tag{4.17}$$

Since $\mathrm{Re}(c_0) < 0$, it follows for $T \to \infty$, and for any $\mu > 0$, that the eigenvalues approach the origin from the unstable right-half plane $\mathrm{Re}(\lambda) > 0$. The eigenvalue in (4.17) with $n = 0$ is real and tends to the origin as $T \to +\infty$.

Finally, we can readily show from (4.11) that, for any $\mu > 0$, there are exactly two real eigenvalues on the interval $0 < \lambda < \sigma_0$, where $\sigma_0 \approx 1.648$ is the principal eigenvalue of L_0, whenever T is sufficiently large.

5. Hopf Bifurcations With Both Inhibitor and Activator Delayed Kinetics. In this section we consider the GM model with exponent set $(p, q, m, s) = (2, 1, 2, 0)$ under the effect of reaction kinetic delays in both the activator and

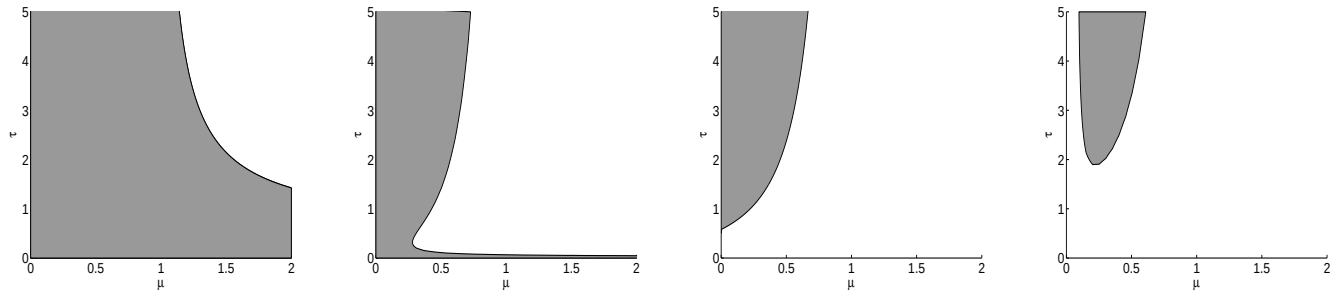

Fig. 4.4: Cross-sections of the stability region for the synchronous mode in the τ versus μ plane for four values of the delay; $T = 0$ (left); $T = 0.35 < T^f$ (left middle); $T \approx T^f$ (right middle); $T = 0.4 \in (T^f, T_{\max})$ (right). Here $T^f \approx 0.379$ is the Hopf bifurcation value of the delay when $\tau = 0$, which is independent of μ.

the inhibitor. For an arbitrary exponent set, the NLEP for a one-spike solution for the 1-D shadow problem and the infinite-line problem have been derived in (2.4) and (3.8), respectively. For the case of an M-spot pattern with $M > 1$ on a finite domain in the regime $D = D_0/\nu \gg 1$, studied in §4 for the exponent set $(p, q, m, s) = (2, 1, 2, 0)$ assuming only a delay in the inhibitor, the NLEP is obtained by replacing $L_0\Phi$ and $e^{-\lambda T}$ in (4.1) with $L_T\Phi$ and $e^{-2\lambda T}$, respectively.

For the exponent set $(p, q, m, s) = (2, 1, 2, 0)$, all these different NLEPs correspond to special cases of a more general NLEP, formulated in terms of the delayed local operator $L_T\Phi \equiv \Delta_\rho\Phi - \Phi + 2we^{-\lambda T}\Phi$, as

$$L_T\Phi - \tilde{\chi}(\tau\lambda)e^{-2\lambda T}w^2\frac{\int_0^\infty \rho^{N-1}w\Phi\,d\rho}{\int_0^\infty \rho^{N-1}w^2\,d\rho} = \lambda\Phi\,, \qquad 0 < \rho < \infty\,; \qquad \Phi'(0) = 0\,, \quad \Phi \to 0 \quad \text{as} \quad \rho \to \infty\,, \tag{5.1a}$$

where $w(\rho)$ is the ground-state solution obtained by setting $p = 2$ in (2.31). In (5.1a), $\tilde{\chi}$, which depends only on the product $\tau\lambda$, and the dimension N, with $N = 1, 2$, can be chosen to correspond to one of our NLEPs as follows:

$$\tilde{\chi} \equiv \frac{2}{1+\tau\lambda}\,, \quad N = 1, 2\,, \ \text{(N-D shadow problem)}\,; \qquad \tilde{\chi} = \frac{2}{\sqrt{1+\tau\lambda}}\,, \quad N = 1\,, \ \text{(1-D infinite-line problem)}\,; \tag{5.1b}$$

$$\tilde{\chi} \equiv \frac{2}{1+\mu}\,, \quad N = 2\,, \quad \text{(2-D async)}\,; \qquad \tilde{\chi} \equiv \frac{2}{1+\mu}\left(\frac{1+\mu+\tau\lambda}{1+\tau\lambda}\right), \quad N = 2\,, \quad \text{(2-D sync)}\,. \tag{5.1c}$$

In (5.1c), the two choices of $\tilde{\chi}$ correspond to either the asynchronous and synchronous modes of instability for an M-spot solution in 2-D. In this context, $\mu \equiv 2\pi M D_0/|\Omega|$, as was defined in (4.2b).

It is readily shown that any unstable eigenvalue of (5.1) must be a root of $g(\lambda) = 0$, where

$$g(\lambda) = \frac{e^{2\lambda T}}{\tilde{\chi}(\tau\lambda)} - \mathcal{F}_T(\lambda)\,; \qquad \mathcal{F}_T(\lambda) \equiv \frac{\int_0^\infty \rho^{N-1}w\left[(L_T-\lambda)^{-1}w^2\right]\,d\rho}{\int_0^\infty \rho^{N-1}w^2\,d\rho}\,. \tag{5.2}$$

By setting $g(i\lambda_{IH}) = 0$, where $\lambda_{IH} > 0$, we obtain a 2×2 nonlinear system for the Hopf bifurcation values τ and λ_{IH} at a particular value of the delay $T \geq 0$. By using Newton's method on this system, in Fig. 5.1 we plot the numerically computed Hopf bifurcation boundary in the τ versus T plane for both the 1-D shadow problem and the infinite-line problem. By comparing Fig. 5.1 and Fig. 1.1, we conclude that the stability boundaries for the case of only inhibitor delay are qualitatively rather similar to those that occur when the delay arises in both the activator and inhibitor.

It it is intractable analytically to determine the Hopf bifurcation boundaries for the NLEP (5.1). However, under certain conditions described below, we can show that there must be a Hopf bifurcation value of the delay T. To do so, we first prove the following lemma that characterizes the behavior of certain eigenvalues of the NLEP (5.1a) for $T \gg 1$:

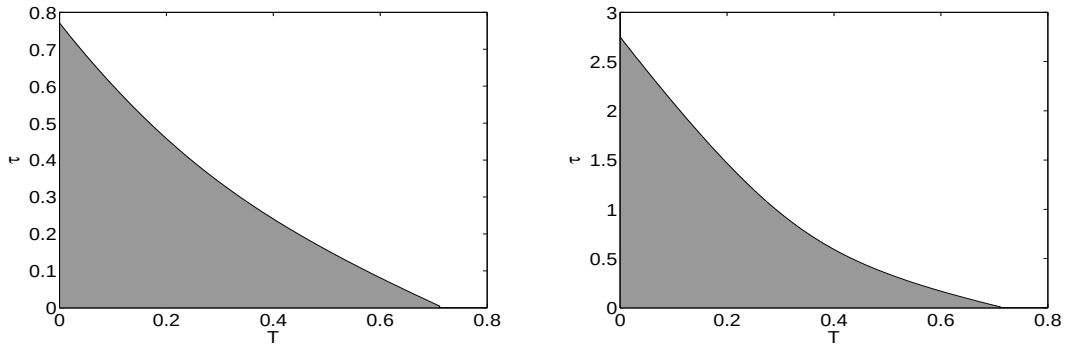

Fig. 5.1: The effect of delay in both the activator and inhibitor. The stable shaded region in the τ versus T plane for a one-spike solution to the 1-D shadow GM problem (left figure) and for the infinite-line problem (right figure). The GM exponents are $(p, q, m, s) = (2, 1, 2, 0)$. The Hopf bifurcation boundaries of the shaded regions are computed using Newton's method on (5.2) with $\lambda = i\lambda_{IH}$. These plots are similar to those shown in Fig. 1.1 with only a delay in the inhibitor kinetics.

Lemma 5.1. *Consider the NLEP (5.1a) where the multiplier $\tilde{\chi}(\tau\lambda)$ has the asymptotic behavior $\tilde{\chi}(\tau\lambda) \sim \tilde{\chi}_0 + \tau\lambda\tilde{\chi}_1 + \cdots$, as $\lambda \to 0$, where $\tilde{\chi}_0 > 0$. Then, for $T \gg 1$, the eigenvalues of (5.1a) near the origin have the limiting asymptotics*

$$\lambda \sim \frac{c_0}{T} + \frac{c_1}{T^2} + \cdots, \qquad c_1 \equiv \frac{c_0}{2}\left(e^{-c_0} - 1\right)^{-1}\left(\frac{I_{1T}}{I_{2T}} + \tau\tilde{\chi}_1 e^{-2c_0}\right), \tag{5.3a}$$

where c_0 and the integral ratio I_{1T}/I_{2T} satisfy

$$\tilde{\chi}_0 e^{-2c_0} - 2e^{-c_0} + 1 = 0\,; \qquad \frac{I_{1T}}{I_{2T}} \equiv \frac{\int_0^\infty \rho^{N-1} w\Psi^\star\, d\rho}{\int_0^\infty \rho^{N-1} w^2\Psi^\star\, d\rho}\,. \tag{5.3b}$$

Here Ψ^* is the solution to the following adjoint problem on $0 < \rho < \infty$;

$$\Delta_\rho\Psi^\star - \Psi^\star + 2we^{-c_0}\Psi^\star - \tilde{\chi}_0 e^{-2c_0} w\frac{\int_0^\infty \rho^{N-1}w^2\Psi^\star\, d\rho}{\int_0^\infty \rho^{N-1}w^2\, d\rho} = 0\,; \qquad \Psi^\star_\rho(0) = 0\,, \quad \Psi^\star \to 0 \quad as \quad \rho \to \infty\,. \tag{5.3c}$$

Proof. We set $\lambda T = c$ with $T \gg 1$ and $\lambda \ll 1$, and use $\tilde{\chi}(\lambda) \sim \tilde{\chi}_0 + \tau\lambda\tilde{\chi}_1 + \cdots$ as $\lambda \to 0$ to obtain

$$\Delta_\rho\Phi - \Phi + 2we^{-c}\Phi - e^{-2c}\left(\tilde{\chi}_0 + \frac{c\tau}{T}\tilde{\chi}_1 + \cdots\right) w^2\frac{\int_0^\infty \rho^{N-1}w\Phi\, d\rho}{\int_0^\infty \rho^{N-1}w^2\, d\rho} = \frac{c}{T}\Phi + \cdots\,. \tag{5.4}$$

We then expand $c = c_0 + c_1/T + \cdots$ and $\Phi = \Phi_0 + \Phi_1/T + \cdots$, and substitute these expressions into (5.4). Upon equating powers of $1/T$, and defining the operator $L_c\Phi$ by $L_c\Phi \equiv \Delta_\rho\Phi - \Phi + 2we^{-c_0}\Phi$, we get

$$L_c\Phi_0 - \tilde{\chi}_0 e^{-2c_0} w^2\frac{\int_0^\infty \rho^{N-1}w\Phi_0\, d\rho}{\int_0^\infty \rho^{N-1}w^2\, d\rho} = 0\,, \tag{5.5a}$$

$$L_c\Phi_1 - \tilde{\chi}_0 e^{-2c_0} w^2\frac{\int_0^\infty \rho^{N-1}w\Phi_1\, d\rho}{\int_0^\infty \rho^{N-1}w^2\, d\rho} = e^{-2c_0}\left(c_0\tau\tilde{\chi}_1 - 2c_1\tilde{\chi}_0\right) w^2\frac{\int_0^\infty \rho^{N-1}w\Phi_0\, d\rho}{\int_0^\infty \rho^{N-1}w^2\, d\rho} + \left(c_0 + 2e^{-c_0}c_1 w\right)\Phi_0\,. \tag{5.5b}$$

Now since $L_c w = w^2\left(-1 + 2e^{-c_0}\right)$, we obtain from (5.5a) that $\Phi_0 = w$ provided that c_0 satisfies (5.3b). Then, the solvability condition for (5.5b) yields that $e^{-2c_0}\left(c_0\tau\tilde{\chi}_1 - 2c_1\tilde{\chi}_0\right) I_{2T} + 2e^{-c_0}c_1 I_{2T} + c_0 I_{1T} = 0$. Upon solving for c_1, and using $2e^{-c_0} = \tilde{\chi}_0 e^{-2c_0} + 1$ from (5.3b), we obtain the expression for c_1 in (5.3a). □

We now show from (5.3a) that for $T \gg 1$ there are many eigenvalues near the origin in the right-half plane $\mathrm{Re}(\lambda) > 0$ whenever $\tilde{\chi}_0 > 1$. To establish this, we observe that (5.3b) is a quadratic in e^{-c_0}, which can be solved to yield

$$\lambda \sim c_0/T\,, \qquad c_0 = \ln\tilde{\chi}_0 + i\left[\tan^{-1}\left(\sqrt{\tilde{\chi}_0 - 1}\right) + 2n\pi\right] + \cdots\,, \qquad n = 0, \pm 1, \pm 2, \ldots\,. \tag{5.6}$$

Therefore, if $\tilde{\chi}_0 > 1$, we have $\mathrm{Re}(c_0) > 0$, and consequently $\mathrm{Re}(\lambda) > 0$ for $T \gg 1$.

Finally, we establish for (5.1a) that, for fixed $\tau < \tau_H^0$ and $\tilde{\chi}_0 > 1$, there must be a Hopf bifurcation whenever the delay T is large enough. Here $\tau = \tau_H^0$ is the Hopf bifurcation threshold for (5.1a) when there is no delay $T = 0$. Qualitatively, this result corresponds to taking a horizontal slice at a fixed τ through the stability diagrams of Fig. 5.1. From (5.1b) we conclude that $\tilde{\chi}_0 = 2 > 1$ for both the shadow and infinite-line problems. From (5.1c), we also have $\tilde{\chi}_0 = 2 > 1$ for all $\mu > 0$ for the synchronous mode. However, for the asynchronous mode, we have $\tilde{\chi}_0 > 1$ only when $0 < \mu < 1$.

To establish this result we proceed as follows. We first observe that eigenvalues for (5.1a) can never cross through the origin $\lambda = 0$ as either τ or T increases, owing to the fact that the eigenvalues depend on the product λT and $\lambda\tau$. Next, we recall from [24] that all eigenvalues of the NLEP (5.1a) satisfy $\mathrm{Re}(\lambda) < 0$ when $\tau = 0$ and $T = 0$ if and only if $\tilde{\chi}_0 > 1$. Fixing $T = 0$, and assuming $\tilde{\chi}_0 > 1$, then, as we have shown for the different choices (5.1b) and (5.1c) in §2–4, (5.1a) has a Hopf bifurcation at some value $\tau = \tau_H^0 > 0$, with $\mathrm{Re}(\lambda) < 0$ for $0 < \tau < \tau_H^0$. Finally, if we take $\tilde{\chi}_0 > 1$ and fix τ in $0 < \tau < \tau_H^0$, then for sufficiently large delay T we have from (5.6) that many eigenvalues tend to the origin as $T \to \infty$. Therefore, if the eigenvalue paths are continuous in T, then there must be an intermediate value of the delay T at which a Hopf bifurcation first occurred. The outline of a rigorous proof of this statement is sketched as follows:

Remark 5.1. *We follow the arguments of [3] to establish the existence of Hopf bifurcation. We first check the Fredholm properties of the eigenvalue problem (5.1a). Note that the map* $\Phi \to 2we^{-\lambda T}\Phi - \tilde{\chi}(\tau\lambda)e^{-2\lambda T}w^2\frac{\int_0^\infty \rho^{N-1}w\Phi d\rho}{\int_0^\infty \rho^{N-1}w^2 d\rho}$ *is a relatively compact operator of* $H^2(R^N)$ *into* $L^2(R^N)$ *since* w *is exponentially decaying. Hence* $L_T - \lambda$ *is Fredholm if and only if* $\Delta - (1+\lambda)$ *is Fredholm and this is true as long as* $\lambda > -1$ *or* $Im(\lambda) \neq 0$*. Thus, the operator*

$$L_T\Phi - \tilde{\chi}(\tau\lambda)e^{-2\lambda T}w^2\frac{\int_0^\infty \rho^{N-1}w\Phi d\rho}{\int_0^\infty \rho^{N-1}w^2 d\rho} - \lambda\Phi\,,$$

is Fredholm of index zero if $\lambda > -1$ *or* $Im(\lambda) \neq 0$*. Since* $|e^{-\lambda T}| \leq 1$ *for* $Re(\lambda) \geq 0$*, we conclude that all eigenvalues of (5.1a) lie on the left half plane* $Re(\lambda) \leq K$ *for some* $K > 0$*, independent of* $T > 0$*. This implies the analyticity of the operator for* $-1 < Re(\lambda) \leq K$*. The analyticity of the operator, the Fredholm property and a classical theorem of Gokhberg and Krein [2, Theorem 3.6] imply that the eigenvalues of (5.1a) in the region* $-1 < Re(\lambda) < K$ *are isolated. This then implies that the eigenvalue paths are continuous in the delay parameter* T*. We now choose the path containing the lowest branch in (5.6) and continue this branch in decreasing* T*.*

Next, we consider the limiting behavior as $T \to \infty$ of any eigenvalue near the origin when $\tilde{\chi}_0$ satisfies $0 < \tilde{\chi}_0 < 1$. From (5.1c) the condition $0 < \tilde{\chi}_0 < 1$ holds only for the asynchronous mode when $\mu > 1$. We define $y = e^{-c_0}$, and write the quadratic equation (5.3b) for e^{-c_0} as $\mathcal{H}(y) \equiv \tilde{\chi}_0 y^2 - 2y + 1 = 0$. We calculate that $\mathcal{H}'(y) = 0$ at $y = 1/\tilde{\chi}_0 > 1$, and that $\mathcal{H}\left(1/\tilde{\chi}_0\right) = 1 - 1/\tilde{\chi}_0 < 0$. Moreover, we calculate that $\mathcal{H}(0) > 0$, $\mathcal{H}(1) = \tilde{\chi}_0 - 1 < 0$, and $\mathcal{H}(y) \to +\infty$ as $y \to +\infty$. It follows that $\mathcal{H}(y) = 0$ has two roots $y_\pm$, which satisfy $0 < y_- < 1$ and $y_+ = 1/\tilde{\chi}_0 > 1$. Only for the smaller of the two roots, for which $c_{0-} \equiv -\ln y_- > 0$ since $0 < y_- < 1$, will we have $\mathrm{Re}(\lambda) > 0$.

Finally, we remark on an open issue regarding the boundedness of the eigenvalues of the NLEP as T is increased.

Remark 5.2. *It is easy to prove that if* $Re(\lambda) \equiv \lambda_R \geq 0$*, then* $\lambda_R = \mathcal{O}\left(1/T\right)$ *as* $T \to \infty$*. In fact, if not, we would have* $|e^{-\lambda T}| \to 0$ *which can be easily excluded by (5.1a). However, it is unclear if there holds*

$$Im(\lambda) \equiv \lambda_I = \mathcal{O}\left(1/T\right)\,,$$

as $T \to \infty$. Indeed let $\lambda T = c_T + i(b_I + 2n\pi)$ where $0 \le b_I < 2\pi$. Assuming for a subsequence of $T_n \to +\infty$ that there holds $c_T \to c_0, b_T \to b_0, e^{-\lambda T} \to e^{-c_0 - ib_0} = \mu_0$ and $\frac{2n\pi}{T} \to a_0$, then we obtain the following limiting NLEP, as $T \to +\infty$

$$\Delta\Phi - \Phi + 2w\mu_0\Phi - \tilde{\chi}(\tau i a_0)\mu_0^2 w^2 \frac{\int_0^\infty \rho^{N-1} w\Phi d\rho}{\int_0^\infty \rho^{N-1} w^2 d\rho} = i a_0 \Phi\,.$$

The existence of eigenvalues of this problem would imply the existence of another branch of eigenvalues with $\lambda = \lambda_R + i\lambda_I, \lambda_R = O(\frac{1}{T}), \lambda_I = a_0 + O(\frac{1}{T})$. We leave this as an open question.

6. Discussion. Motivated by the computational studies (cf. [5], [13], [14], [17]) of pattern formation in RD systems with a time-delay in the reaction-kinetics, modeling gene expression time delays, we have analyzed the linear stability of spike solutions to various limiting forms of the GM RD model with delayed reaction-kinetics in both 1-D and 2-D domains. Our analysis has provided phase diagrams in parameter space where such solutions are linearly stable.

When the delay occurs only in the inhibitor kinetics, one of our main conclusions is that if the delay T exceeds a threshold, the steady-state spike solution is unconditionally unstable. Comparison with full numerical results in 1-D suggests that large-scale oscillations, indicative of a subcritical Hopf bifurcation, occur just beyond the Hopf bifurcation boundary. Such uncontrolled oscillations, representing a global breakdown of a robust stable patterning mechanism, were observed in the numerical studies of [5], [13], and [14] for the GM and some related models. A second main conclusion of our study is that our detailed and explicit analysis of spike stability for the special subrange of GM exponents for which the NLEP is explicitly solvable is actually representative of the more general case. More specifically, we showed that qualitatively identical conclusions regarding the stability of a spike hold for more general GM exponent sets, including the prototypical GM model where $(p, q, m, s) = (2, 1, 2, 0)$ in (1.1). Finally, although we have primarily focused on the case where only the inhibitor kinetics has a time-delay, in §5 we have also shown that qualitatively similar results occur when both the activator and inhibitor reaction-kinetics have a time delay. In particular, for this latter case where the study of the NLEP is intractable analytically, we have determined the Hopf bifurcation boundary numerically and have shown analytically, for various limiting forms of the GM model, that a Hopf bifurcation must occur as the delay increases.

We now briefly discuss a few possible extensions of this study. Firstly, from a mathematical viewpoint, it would be interesting to investigate whether the Hopf bifurcation due to delayed reaction-kinetics is typically subcritical, confirming the numerical observations in [13] and §3.3, and therefore can lead to uncontrolled oscillations of the spike amplitude near the Hopf bifurcation boundary. Secondly, our analysis has been restricted to determining the linear stability of spike solutions on an $\mathcal{O}(1)$ time-scale, as characterized by the spectrum of an NLEP. In addition, it would be interesting to determine the effect of a time-delay in the reaction-kinetics on the small eigenvalues of order $\mathcal{O}(\epsilon^2)$ (cf. [11]) in the linearization of the steady-state spike pattern. Moreover, it is an open problem to derive and then analyze an ODE with time-delay characterizing the slow dynamics of a spike for the finite-domain problem under delayed reaction-kinetics.

From a modeling viewpoint, the analysis herein has shown that there is a rather restricted range of the delay T in the GM reaction-kinetics that can lead to linearly stable steady-state spike patterns. Given that time-delays in reaction-kinetics are well-motivated biologically as a result of time lags needed for gene expression (cf. [5], [13], [14], [15], [17]), a natural modeling question is how to incorporate time-delays in the reaction-kinetics but still maintain robustly stable spatial patterning. Although some such possible improved models are discussed in (cf. [5], [13], [14], [15], [17]), it would also be interesting to explore the effect of time-delays on a new class of 2-D quorum-sensing models (cf. [18], [8]) for which spatially localized signaling compartments, undergoing nonlinear kinetics, are coupled through a 2-D bulk diffusion field. For a related class of 2-D models with small signaling compartments, it has been shown recently in [9] that time-delays can lead to stable temporal oscillations.

Acknowledgements. M. J. Ward and J. Wei were supported by NSERC (Canada). Nabil Fadai was supported under the NSERC-USRA program in the summer of 2013.

REFERENCES

[1] S. Chen, J. Shi, *Global attractivity of equilibrium in Gierer-Meinhardt system with activator production saturation and gene expression time delays*, Nonlinear Analysis: Real World Applic., **14**(4), (2013), pp. 1871–1886.
[2] S. Chen, J. Shi, J. Wei, *Time delay-induced instabilities and Hopf bifurcations in general reaction-diffusion systems*, J. Nonl. Sci., **23**(1), (2013), pp. 1–38.
[3] E. N. Dancer, *On stability and Hopf bifurcations for chemotaxis systems*, Meth. Applic. of Anal., **8**(2), (2001), pp. 245–256.
[4] A. Doelman, R. A. Gardner, T. Kaper, *Large stable pulse solutions in reaction-diffusion equations*, Indiana U. Math. Journ., **50**(1), (2001), pp. 443-507.
[5] E. A. Gaffney, N. A. M. Monk, *Gene expression time delays and Turing pattern formation systems*, Bull. Math. Bio., **68**, (2006), pp. 99–130.
[6] A. Gierer, H. Meinhardt, *A theory of biological pattern formation*, Kybernetik, **12**, (1972), pp. 30–39.
[7] I. Gokhberg, M. Krein, *Fundamental theorems on deficiency indices, root numbers and indices of linear operators*, Amer Math Soc. Transls., **2**(13), (1960), pp. 185-264.
[8] J. Gou, M. J. Ward, *Asymptotic analysis of a 2-D model of dynamically active compartments coupled by bulk diffusion*, accepted, J. Nonl. Sci. (2015), (37 pages).
[9] D. Iron, C. Levy, *Dynamics and stability of a three-dimensional model of cell signal transduction with delay*, Nonlinearity, **28**(7), (2015), pp. 2515–2554.
[10] D. Iron, M. J. Ward, *A metastable spike solution for a non-local reaction-diffusion model*, SIAM J. Appl. Math., **60**(3), (2000), pp. 778-802.
[11] D. Iron, M. J. Ward and J. Wei, *The stability of spike solutions to the one-dimensional Gierer-Meinhardt model*, Physica D, **150**(1-2), (2001), pp. 25–62.
[12] T. Kolokolnikov, M. Ward, J. Wei, *The stability of steady-state hot-spot patterns for a reaction-diffusion model of urban crime*, DCDS-B, **19**(5), (2014), pp. 1373-1410.
[13] S. Lee, E. A. Gaffney, N. A. M. Monk, *The influence of gene expression time delays on Gierer-Meinhardt pattern formation systems*, Bull. Math. Bio., **72**(8), (2010), pp. 2139–2160.
[14] S. Lee, E. A. Gaffney, *Aberrant behaviors of reaction-diffusion self-organization models on growing domains in the presence of gene expression time delays*, Bull. Math. Bio., **72**(8), (2010), pp. 2161-2179.
[15] S. Lee, E. A. Gaffney, R. E. Baker, *The dynamics of Turing patterns for morphogen-regulated growing domains with cellular response delays*, Bull. Math. Bio., **73**, (2011), pp. 2527–2551.
[16] C. S. Lin, W. M. Ni, I. Takagi, *Large amplitude stationary solutions to a chemotaxis system*, J. Diff. Eq., **72**(1), (1988), pp. 1-27.
[17] P. Maini, T. Woolley, R. E. Baker, E. A. Gaffney, S. Lee, *Turing's model for biological pattern formation and the robustness problem*, Interface Focus, **2012**(2), (2012), pp. 487–496.
[18] J. Müller, C. Kuttler, B. A. Hense, M. Rothballer, A. Hartmann, *Cell-cell communication by quorum sensing and dimension-reduction*, J. Math. Biol., **53**(4), (2006), pp. 672–702.
[19] Y. Nec, M. J. Ward, *An explicitly solvable nonlocal eigenvalue problem and the stability of a spike for a class of reaction-diffusion systems*, Math. Model. of Nat. Phenom., **8**(2), (2013), pp. 55–87.
[20] A. Turing, *The Chemical Basis of Morphogenesis*, Phil. Trans. Roy. Soc. B, **327**, (1952), pp. 37-72.
[21] H. Van der Ploeg, A. Doelman, *Stability of spatially periodic pulse patterns in a class of singularly perturbed reaction-diffusion equations*, Indiana Univ. Math. J., **54**(5), (2005), pp. 1219-1301.
[22] M. J. Ward, J. Wei, *Hopf bifurcation of spike solutions for the shadow Gierer-Meinhardt model*, Europ. J. Appl. Math., **14**(6), (2003), pp. 677–711.
[23] M. J. Ward, J. Wei, *Hopf bifurcations and oscillatory instabilities of spike solutions for the one-dimensional Gierer-Meinhardt model*, J. Nonlinear Science, **13**(2), (2003), pp. 209–264.
[24] J. Wei, *On single interior spike solutions for the Gierer-Meinhardt system: uniqueness and stability estimates*, Europ. J. Appl. Math., **10**(4), (1999), pp. 353-378.
[25] J. Wei, *Existence and stability of spikes for the Gierer-Meinhardt system*, book chapter in *Handbook of Differential Equations, Stationary Partial Differential Equations*, Vol. 5 (M. Chipot ed.), Elsevier, (2008), pp. 489–581.
[26] J. Wei, M. Winter, *Spikes for the two-dimensional Gierer-Meinhardt system: the weak coupling case*, J. Nonlinear Sci., **11**(6), (2001), pp. 415–458.